Atmos. Chem. Phys., 26, 12813–12836, 2026
https://doi.org/10.5194/acp-26-12813-2026

Atmospheric Chemistry and Physics
Open Access
EGU

Unraveling the chemical structures and sources of biomass-derived organic aerosols through a year-long offline analysis in Hyytiälä, Finland

Qianzhe Sun[1], Ruichen Zhou[2], Sho Ohata[2], Chiaki Shirota[3], Tuukka Petäjä[4], Ilona Jaakkola[4], Lauri Ahonen[4], Markku Kulmala[4], and Michihiro Mochida[1,2]

[1]Graduate School of Environmental Studies, Nagoya University, Nagoya, Japan
[2]Institute for Space-Earth Environmental Research, Nagoya University, Nagoya, Japan
[3]Murata Keisokuki Service Co., Ltd., Yokohama, Japan
[4]Institute for Atmospheric and Earth System Research (INAR)/Physics, University of Helsinki, Helsinki, Finland

Correspondence: Michihiro Mochida (mochida@isee.nagoya-u.ac.jp)

Received: 24 February 2026 – Discussion started: 16 March 2026
Revised: 24 August 2026 – Accepted: 24 August 2026 – Published: 11 September 2026

Abstract. Biomass-burning OA (BBOA) and biogenic secondary OA (BSOA), both originating from biomass but from different pathways, still lack comprehensive and quantitative understanding, which limits assessments of their environmental impacts. In this study, source-resolved OAs including BBOA and BSOA in a European boreal forest were characterized by the offline use of an aerosol mass spectrometer (AMS), with improved chemical resolution offered by polarity-based fractionation. OA extract solutions were prepared according to polarity as high-polarity water-soluble organic matter, humic-like substances, and water-insoluble organic matter, and their abundances and chemical structures were analyzed by off-line high-resolution AMS analysis. Quantitative analysis revealed an annual OA concentration of $1.24 \pm 0.75\,\mu g\,m^{-3}$, with lower concentrations in winter and higher in summer. A 5-factor source apportionment solution was obtained from positive matrix factorization (PMF) of the mass spectra of the three fractions. CHN-family ions were found to be indicative of BBOA, whereas $C_5H_6O^+$, $C_7H_9O_3^+$ and $C_9H_{13}O_4^+$ were identified as potential tracers for BSOA; they lead the identification of BBOA- and BSOA-like factors. Combustion-related organic aerosol (CROA) factor, related to aged fossil fuel combustion and aged biomass material combustion, was also identified. Different PMF factors exhibited differences in water solubility, with relatively water-insoluble characteristics of compounds containing CROA aromatic structures. This study highlights the usefulness of polarity-resolved factor analysis in understanding diverse OA sources and opens the door for the characterization of climate- and air-quality-related properties of BBOA and BSOA.

1 Introduction

Biomass-burning organic aerosol (BBOA) and biogenic secondary organic aerosol (BSOA) are two types of organic aerosols (OAs) that originate from biomass sources, but have vastly different formation pathways. Biomass burning is among the greatest sources of atmospheric OAs and has become a global environmental concern (Simoneit, 2002; Laskin et al., 2009). The chemical composition and physicochemical properties of BBOA are highly dependent on the type of biomass burned. For instance, fresh biomass emissions from wildfires differ substantially from those associated with agricultural residues, fallen leaves, or decaying wood (Ma et al., 2024). BSOA originate from the atmospheric oxidation of biogenic volatile organic compounds (BVOCs), whose emission strength and chemical profiles are strongly influenced by vegetation type and meteorological conditions (Qin et al., 2018; Müller et al., 2020). Globally,

terrestrial vegetation emits more than 1 Pg of BVOCs annually, making it a dominant source of secondary organic aerosols (Guenther et al., 2012; Zheng et al., 2023). The separate quantification of BBOA and BSOA is required to understand the respective effects of these two types of OAs on climate and air quality through their distinct properties. The effect based on their light absorptivity is a representative example to be studied, as BBOA is considered a major source of light-absorbing OA (Li et al., 2025; Afsana et al., 2022), whereas BSOA is regarded as weakly light-absorbing (Deng et al., 2019).

A single, definitive technique for distinguishing between BBOA and BSOA has yet to be established, since most available methods have inherent limitations as well as advantages. For example, radiocarbon (^{14}C) analysis is widely used to distinguish between fossil fuel and modern carbon sources, but it is not effective for differentiating BSOA from BBOA (Dusek et al., 2017; Szidat et al., 2006). The organic carbon (OC)-to-elemental carbon (EC) ratio can be used to estimate the abundance of primary organic carbon (POC) and secondary organic carbon (SOC), but it cannot serve as a robust approach for source apportionment (Gelencsér et al., 2007; Dusek et al., 2017). Molecular-tracer-based methods, which use source-specific molecular markers, are among the most widely applied approaches and enable the quantification of various compound classes (Cheng et al., 2021; Haque et al., 2023; Gilardoni et al., 2011). The chemical mass balance (CMB) model is a source apportionment technique that relies on source profiles and molecular tracer concentrations, but the apportionment of SOAs using CMB remains highly uncertain, partly owing to the atmospheric degradation of organic tracers and the challenges associated with the representativeness of the source profiles used (Yin et al., 2015; Srivastava et al., 2018; Schauer et al., 1996). The combination of aerosol mass spectrometer (AMS) measurements and positive matrix factorization (PMF) has also been widely applied for source apportionment of OAs in online studies (Corrigan et al., 2013; Ulbrich et al., 2009a). As a receptor model, PMF resolves measured mass spectral data into different factors that represent distinct source profiles and their temporal contributions (Zhang et al., 2011). However, distinguishing BBOA and BSOA generally remains challenging in online AMS studies without additional techniques such as FT-IR or NMR (Liu et al., 2016; Zhang et al., 2024; Finessi et al., 2012). The above methods are often jointly applied in studies aiming to distinguish between BBOA and BSOA, as each has its own advantages and limitations.

The offline application of high-resolution AMS (HR–AMS) measurement with PMF, which has emerged in recent years (Zhou et al., 2021), is a possible new approach to advance the source apportionment of OA. Various methods to extract chemical components from aerosol samples collected on filters have been developed for offline AMS analysis, including the use of water (Duarte and Duarte, 2011), ethanol (Cheng et al., 2016), and ethyl acetate (Mihara and Mochida, 2011) as solvents for extraction. Recently, solid-phase extraction (SPE) to isolate fractions with distinct polarities has been applied in offline AMS studies, allowing for a detailed investigation of OA properties with high extraction efficiency (Chen et al., 2016b). Humic-like substances (HULIS) comprise a subset of water-soluble organic matter (WSOM) isolated using SPE and are named for their resemblance to terrestrial and aquatic humic and fulvic acids (Lin et al., 2010). Compared with HULIS, the remaining water-soluble fraction, high-polarity WSOM (HP-WSOM), is generally considered to have lower light absorptivity and greater hygroscopicity (Lin et al., 2010; Zhang et al., 2022; Gysel et al., 2004). Water-insoluble organic matter (WISOM) consists of relatively high-molecular-weight compounds (Chen et al., 2016b) and has strong light absorption (Chen et al., 2017). Previous studies using offline HR–AMS analysis have shown that the polarity of different OA fractions (HP-WSOM, HULIS, and WISOM) is positively correlated with the O/C ratio and that each fraction is dominated by distinct PMF factors (Zhou et al., 2021). Compared with conventional online AMS analysis, the addition of polarity-based fractionation improves the chemical resolution and may aid in the identification and quantification of OA sources, including BBOA and BSOA.

In conventional AMS studies, various mass spectrometric ion tracers have been adopted to differentiate between BBOA and BSOA. Compared with the molecular-tracer-based approach, fragment ions from AMS analysis may retain structural information of compounds including those that are not identified and quantified in molecular-based approach. An example of an ion tracer is $C_5H_6O^+$ (m/z 82), which has been recognized as a highly specific and quantitative tracer for isoprene-derived SOAs (Hu et al., 2015). In contrast, monoterpene-derived SOAs generally produce nonspecific hydrocarbon fragments such as $C_5H_7^+$, $C_6H_9^+$, and $C_7H_7^+$, and reliable fragment ion tracers have yet to be firmly established. BBOA are typically characterized by the presence of levoglucosan, a cellulose pyrolysis product and tracer for fresh biomass burning emissions (Jolleys et al., 2015). Further, fragment ions $C_2H_4O_2^+$ (m/z 60) and $C_3H_5O_2^+$ (m/z 73) are commonly associated with levoglucosan and have been widely used as markers of fresh BBOA in previous studies (Alfarra et al., 2007; Sun et al., 2016). However, the atmospheric lifetime of levoglucosan is estimated to be short, for example, 0.7–2.2 d under OH radical exposure (Hennigan et al., 2010), making it difficult to detect in air masses transported over long ranges (Zhang et al., 2024). Moreover, alkyl amides and nitriles have been identified as potential tracers for biomass burning. High temperatures during combustion promote the release of ammonia and amines that react with carboxylic acids to form alkyl amides, which can further undergo dehydration to yield alkyl nitriles (Chen et al., 2018; Ratcliff et al., 1974; Simoneit et al., 2003). As a result, nitrogen-containing organic compounds (NOCs) in biomass burning-derived aerosols contribute to the detection of both

CHN and CHON ion groups in AMS analysis (Laskin et al., 2009). In contrast, OAs from biogenic volatile organic compounds (BVOCs), including α-pinene and limonene, primarily generate CHON ions instead of CHN ions through oxidation and nitration processes, as detected by AMS (Laskin et al., 2014). Therefore, CHN family ions detected by AMS may serve as novel tracers for BBOA. The fragment ions obtained via AMS described above are potentially useful for distinguishing between BBOA and BSOA quantitatively and for advancing the characterization of their properties.

In this study, by analyzing the one-year filter samples collected at the Station for Measuring Ecosystem-Atmosphere Relations (SMEAR II) in the Hyytiälä forest, we differentiated between BBOA and BSOA in OAs and characterized their chemical structural characteristics through offline AMS analysis with increased chemical resolution by polarity-based fractionation. The Hyytiälä SMEAR II station is a rural site with low anthropogenic influence and strong biogenic emissions (Kulmala et al., 2001; Petäjä et al., 2021). The SMEAR II station is located in the boreal forest region of Fennoscandia, where Scots pine, Norway spruce, birches, and aspen are among the main forest-forming tree species (Kuuluvainen and Aakala, 2011; Ronold et al., 2026; Tunved et al., 2006). The forest surrounding the SMEAR II station emits multiple biogenic non-methane VOCs, dominantly monoterpenes (Heikkinen et al., 2021; Hakola et al., 2012). This provides an ideal environment for investigating the chemical structural differences between BBOA and BSOA, as BSOA is difficult to identify and quantify when there are large contributions from BBOA or anthropogenic aerosols, given that BSOA could occur at much lower concentrations and therefore be easily masked by these stronger sources. The OA components in the samples were fractionated into HP-WSOM, HULIS, and WISOM fractions on the basis of their polarity, which is represented by their water solubility and affinity to an SPE column. Each fraction was analyzed by HR–AMS to determine the concentrations and chemical structural characteristics of OAs. PMF-based source apportionment was performed using the HR–AMS spectra, assisted by chemical structural information from methods developed in this study to distinguish between BBOA and BSOA factors. The polarity-based fractionation retains the physicochemical differences among HP-WSOM, HULIS, and WISOM, allowing PMF factors to reflect not only information related to sources but also structural features associated with the fractions with different polarity. Although conventional PMF analysis generally assumes that aerosols from different sources have stable compositions, this assumption may not necessarily apply to AMS-based PMF analysis of OA, because atmospheric aging can modify some molecular structures while preserving other structural features. This study adopted polarity-based fractionation and applied PMF independently to the fraction-resolved spectra. This approach allowed the apportionment of the characteristic structures to OA sources across different OA fractions and to obtain PMF factors that reflect dynamic mixtures of source-related submolecular structures rather than fixed sets of organic compounds. Based on this framework, the analyses were performed to investigate the seasonal variations in OA masses from different sources and how their solubility was influenced by their different chemical structural characteristics. The relative contributions of different OA fractions and the annual average OA concentration from this study were compared with those from other locations.

2 Methodology

2.1 Sample collection

Aerosol samples with diameters smaller than 0.95 µm ($PM_{0.95}$) were collected on quartz fiber filters using a high-volume air sampler (Model 120SL; Kimoto Electric Co., Ltd.) equipped with a cascade impactor (TE-234; Tisch Environmental, Inc.) at SMEAR II (Tarvainen et al., 2005), Hyytiälä Juupajoki, Finland (61°51′ N, 24°17′ E), from July 2021 to June 2022. After one week of collection, aerosol filter samples were transferred to preheated glass jars fitted with Teflon lined screw caps and stored in the dark around −20 °C until analysis. Field blanks were also collected at the sampling site and, after only 10 s of air sampling, were handled in the same manner as the other samples. Detailed sample information is provided in Table S1 in the Supplement. In this study, aerosol samples were collected over one week to obtain sufficient OA mass, and this time scale is also suitable for discussing seasonal scale variations in OA composition. While prolonged filter sampling may introduce some sampling artifacts. For semi-volatile organic compounds, if their atmospheric composition and gas-particle partitioning conditions changed during the one-week sampling period, the compounds already collected on the filter may have re-equilibrated with the air subsequently passing through the filter. As a result, the collected sample may have been influenced, to some extent, more strongly by atmospheric conditions closer to the end of the sampling period. In addition, oxidation or other chemical processes may have occurred on the filter during sampling, potentially altering some reactive organic components. Therefore, compared with results obtained from shorter sampling durations, the OA composition, O/C ratios, and PMF factor distributions reported in this study may have been affected to some extent. This potential effect was not further evaluated in this study.

Located in southern Finland, SMEAR II is surrounded by a boreal coniferous forest extending tens of kilometers to the north and northeast (Hellén et al., 2018). The area is sparsely populated and has limited local anthropogenic pollution sources, primarily household heating and cooking (Äijälä et al., 2017). A small residential and industrial area in Korkeakoski, located 6–7 km southeast of the sampling site, was reported to contain two sawmills and a pellet factory (Heikkinen et al., 2020; Liao et al., 2011;

Ylivinkka et al., 2025). In summer, biogenic aerosols dominate in Hyytiälä, with additional contributions from transported pollution from continental Europe and western Russia, along with occasional influences from biomass burning emissions (Williams et al., 2011). A back trajectory analysis for the period of 1996–2008 indicated that clean air masses from the northwest favor new particle formation, whereas air masses from the southeast transport combustion-related accumulation-mode particles (Riuttanen et al., 2013). Anthropogenic pollution in the area mainly originates from industrial emissions in southern Finland and biomass burning in Russia and Eastern Europe (Yan et al., 2016; Heikkinen et al., 2021).

2.2 Extraction and fractionation

Twenty-four one-week samples, collected around the first and third weeks of each month, were subjected to the extraction of aerosol components. Two circular filter cuts (diameter: 34 mm) were taken from each filter sample for subsequent extraction. First, the punches were extracted three times using approximately 3.3 mL of water and 15 min of ultrasonication in a PTFE-lined glass vial without temperature control, followed by filtration through a 0.2 µm PTFE filter (Millex). Following WSOM extraction, the remaining filters were processed for WISOM extraction through sequential ultrasonication, first with 3 g of methanol, followed by three extractions using ∼ 3.3 g of a dichloromethane/methanol (2 : 1, v/v) mixture (Zhou et al., 2021). Our previous work generally supported the reliability of this ultrasonication-based method, with no clear indication of significant degradation of the extracted organics (Deng et al., 2022).

A portion of the aqueous extract solution (4–6 g) was further processed by solid-phase extraction (SPE) to obtain different fractions (Varga et al., 2001). First, WSOM was acidified to pH 2 using 1 M HCl aqueous solution and passed through an Oasis HLB column (6 cc, 200 mg; Waters) that had been preconditioned with methanol and equilibrated with 0.01 M HCl. Under the acidic condition, polar water-soluble compounds that were not effectively retained by the HLB sorbent passed through the cartridge first. The column was rinsed three times with 0.5 mL of 0.01 M HCl solution, and the resulting effluent was collected as HP-WSOM (Chen et al., 2016a). Then, the HLB column was dried by N_2, after which the species adsorbed on the column were eluted with 6 mL of methanol to obtain HULIS, following the SPE-based operational definition of HULIS (Lin et al., 2010). The details of the SPE extraction method can be found elsewhere (Zhou et al., 2021; Varga et al., 2001). The extraction and SPE workflow was generally performed under normal laboratory lighting conditions. Minor aging during the procedure cannot be fully ruled out, which is not discussed further in the present study.

2.3 HR–AMS measurements and other analyses

The extract solutions of the OA fractions were nebulized using pure compressed air. Aerosols were generated using a home built atomizer equipped with an electrospray nebulizer assembly (G1946-60098 and/or equivalent model; Agilent Technologies, Inc.), to nebulize the solution delivered from a syringe pump without applying a voltage. Approximately 1 mL of the extract solution was loaded into a 5 mL syringe, which was supplied to the atomizer needle continuously. The generated aerosols were then passed through diffusion driers with silica gel and activated carbon to remove solvent vapors. The carrier gas was subsequently replaced with high-purity Ar using a gas exchange device (Argon Gas Flow Unit ARU-03XX, J-Science Lab Co., Ltd., Japan). Finally, the aerosol particles in the Ar flow were analyzed using a high-resolution time-of-flight aerosol mass spectrometer (Aerodyne Research, Inc.). The HR–AMS data were acquired in both V and W modes. The V-mode data were used for to quantify organics, whereas the W-mode data were used for other mass spectral analyses. The AMS data were analyzed using a ToF-AMS Analysis tool kit (Squirrel v1.65G) and a ToF-AMS HR Analysis tool kit (Pika v1.25G) template in Igor Pro (http://cires.colorado.edu/jimenez-group/ToFAMSResources/ToFSoftware/, last access: 23 June 2023). The classification of fragment ions from organics to C_xH_y, $C_xH_yO_1$, $C_xH_yO_{>1}$, $C_xH_yN_z$, $C_xH_yON_z$, $C_xH_yO_{>1}N_z$, H_yO_q, and CS families and the elemental analysis to determine the O/C, H/C, and organic matter-to-organic carbon (OM/OC) ratios were performed using the Pika template. The extract solutions mixed with phthalic acid (PA) as an internal standard were also analyzed using the AMS in the same manner for the quantification of OAs (Mihara and Mochida, 2011).

For quantification, the least squares method was used to deconvolute the unit-mass OA spectrum of the mixture into the spectra of the extracts of OA and phthalic acid, providing the abundance of the extract relative to that of phthalic acid with a known amount (Mihara and Mochida, 2011). The five ions at m/z 28, 44, 50, 76, and 104 were excluded from the quantitative analysis of the WSOM and HP-WSOM samples to increase the fitting accuracy. The detailed rationale for the exclusion of these ions is provided in the Supplement (Text S1). Because of the pH adjustment before SPE, the chemical states of HP-WSOM and HULIS may differ from their original forms in WSOM, potentially affecting their ionization efficiency in AMS. This may have led to fluctuations in the estimated extraction efficiency of SPE (Table S2), with some values slightly exceeding unity. Note that a calculated efficiency greater than unity has also been reported in previous studies (Afsana et al., 2022; Zhou et al., 2021). Comparison of the measured WSOM mass spectra with those reconstructed from the spectra of HP-WSOM and HULIS spectra showed high correlations, with correlation coefficients of 0.996 and 0.989 for the two selected samples,

FIN20Q002 and FIN20Q018, respectively. In addition, the family level distributions of the measured and reconstructed WSOM spectra were highly consistent (Table S8), supporting that the SPE procedure had a minor influence on the AMS results.

Two blank filter samples were extracted and analyzed following the same procedures as the ambient samples. Although the absolute signal intensities of the AMS spectra for OA extracts alone were not used for the quantification of organics (because the possible fluctuation of the nebulizer conditions and the non-linear response of the AMS according to the size distributions of generated particles and the size window of the AMS inlet would affect quantification), we performed a rough comparison between the absolute OA signal intensities (Hz) of the field blanks and those of the samples. For all samples, the blank-to-sample ratios of mean signal intensities were 20.0 % for HP-WSOM, 6.1 % for HULIS, and 4.9 % for WISOM. In contrast, for winter samples, these ratios increased to 46.3 %, 16.6 %, and 13.2 %, respectively. This indicates that the relative influence of blank signals was larger for low-signal samples, particularly for HP-WSOM in winter. Although not directly about the samples used in this study, further details on blank signal characteristics and potential biases associated with size distribution relative to the HR-AMS detection range can be found in Zhou et al. (2021). Note that the phthalic acid internal standard method was not used to assess the blank level, because we suspect that the signal intensities of the OA extracts were too low to support reliable quantification.

Table S3 summarizes the results of duplicate analyses for samples with moderate concentrations. The same extraction procedure, including the SPE step, was applied to evaluate the uncertainties arising from sample handling and instrumental analysis. The maximum relative difference was 17.0 %. For these two samples, the results from the duplicate analyses were averaged and were used in this study.

A total organic carbon analyzer (Model TOC-VCSH, Shimadzu) was used to quantify the water-soluble organic carbon (WSOC) in the samples. The samples for the WSOC analysis were extracted separately from those used for the AMS analysis. The aerosol components on circular filter cuts (diameter: 28 mm) from each filter were extracted into 20 mL of water with two 15 min ultrasonication cycles, followed by filtration through a disposable hydrophilic filter. Organic carbon (OC) and elemental carbon (EC) were analyzed for sample filter cuts (diameter: 8 mm) using a thermal/optical carbon analyzer (Model 2001A, Desert Research Institute) with the thermal/optical reflectance method following the IMPROVE temperature protocol. The abundance of OC was also derived from the HR–AMS analysis as the sum of carbon contents in WISOM, HULIS, and HP-WSOM, where their carbon contents were calculated by dividing their concentrations by their OM/OC ratios. K^+ and SO_4^{2-} were measured using an ion chromatograph (761 Compact IC, Metrohm, Switzerland). For the anion analysis, an SI-90 4E Shodex column (Showa Denko, Tokyo, Japan) was used with an aqueous solution containing Na_2CO_3 and $NaHCO_3$ as the eluent. For the cation analysis, a Shodex IC YK-421 column (Showa Denko) was used with an aqueous solution containing boric acid, tartaric acid, and dipicolinic acid as the eluent.

The quantified HR–AMS results were compared with the OC values from the thermal/optical analysis (Figs. S2 and S3a). The results indicate a strong correlation of the sum of carbon in WISOM, HULIS, and HP-WSOM with the total OC ($r = 0.987$) (Fig. S3a) and the ratio of the latter to the former was 0.75 ± 0.12 (mean $\pm$ SD). To assess the uncertainty associated with low-concentration samples, we further calculated this ratio for winter, the season with low concentrations. The winter mean ratio was 0.72 ± 0.08, indicating that the uncertainty associated with WISOM was not significantly high in winter. The WSOC derived from AMS (HP-WSOM + HULIS) was in good agreement with the WSOC measured by the TOC analyzer, which is represented by a high correlation coefficient ($r = 0.985$; Fig. S3b) and the ratio of the former to the latter of 0.93 ± 0.10 (mean $\pm$ SD). The corresponding winter mean ratio was 0.92 ± 0.10, suggesting that the uncertainty of AMS measurements for HP-WSOM and HULIS in winter was not noticeably higher. These results demonstrate the good accuracy and high extraction efficiency of our quantification method. For TOC, the blank-to-sample ratio of mean values was 2.53 %, whereas for the OC data, the values of the two blank samples were below the detection limit of 0.8 µg-C per filter, which is much lower than the sample loadings (23.4 to 322 µg-C per filter). The results above show that the blank level does not have a significant influence, and we consider that the uncertainty introduced by the absence of the subtraction of the offline AMS procedural blank is acceptable.

Meteorological parameters and atmospheric concentrations of two BVOCs, monoterpenes and MBO (2-methyl-3-buten-2-ol), from 7 July 2021, to 22 June 2022, which were measured at SMEARII and are available in the SmartSMEAR database (Junninen et al., 2009), were averaged for each filter sampling period. The data sources included MBO (16.8 m), monoterpene (8.4 m), SO_2 (16.8 m), acetonitrile (125 m), solar radiation (35 m), and air temperature (16.8 m), all of which were obtained above ground level as quality-checked datasets (Aalto et al., 2025).

2.4 Back trajectory and PSCF analysis

Backward air mass trajectories were calculated using the HYSPLIT model with meteorological input from the NOAA Global Data Assimilation System (GDAS) (Draxler and Hess, 1997; Draxler, 1999; Stein et al., 2015; Draxler and Hess, 1998). back trajectories for the samples from four different seasons are provided in Fig. S7, while those for specific periods P1 and P2 are shown in Fig. S8. Each trajectory started at 500 m above sea level, with one 5 d (120 h) trajectory generated per sampling day at 12:00 UTC.

The potential source contribution function (PSCF) method based on backward trajectory analysis was employed to identify the potential source regions of particle pollution (Bressi et al., 2014; Jeong et al., 2011). PSCF is a trajectory-based receptor model that combines pollutant concentrations observed at the receptor site with the residence of air mass back trajectories in different geographical grid cells, thereby identifying regions that may contribute to elevated pollutant concentrations observed at the receptor site. Hourly trajectories over 120 h periods were computed as inputs of the PSCF for the specific event periods. The hours with high concentrations of aerosols were defined using the 75th percentile of the particle volume concentration calculated using differential mobility particle sizer (DMPS) data for the 100–1000 nm size range, which were measured at SMEARII and are available in the SmartSMEAR database. The 75th percentile was selected because it has been widely used in previous PSCF studies and provides a reasonable balance between selecting characteristic high-concentration data points and retaining sufficient data points for statistically robust PSCF analysis (Fig. S9). The data processing procedures are described in Text S2.

2.5 PMF data processing

To investigate the potential sources of the offline samples, PMF analysis was applied to the HR–AMS mass spectra of the OA fractions. The W-mode HR–AMS data were imported into the Igor PMF template (PMF Evaluation Toolkit v3.08C) for the PMF analysis (Ulbrich et al., 2009a). The mass spectra of all four fractions, HP-WSOM, HULIS, WISOM, and WSOM were treated independently in preparing a single PMF input matrix, their corresponding error matrices were obtained from Pika. This approach was adopted because it allows us to examine whether similar chemical structural characteristics occur across different fractions. Only HR organic ion data were included in the matrix, comprising 1279 ions. Prior to PMF analysis, NaN and zero-only columns were removed. Ions with $\mathrm{SNR} < 0.2$ were excluded, while ions with $0.2 \leq \mathrm{SNR} < 2$ were downweighted by doubling their uncertainties. CO_2^+-related ions (CO_2^+, CO^+, H_2O^+, HO^+, and O^+) were also downweighted to avoid overweighting of duplicated information (Zhang et al., 2005; Ulbrich et al., 2009a). Five PMF solutions with fPeak and seed values of 0 and 1, respectively, were used for further analysis. Detailed results of the stability analysis for the PMF solutions, including the dependence of Q/Q_{expected} on the number of factors, seed, and fPeak values, are provided in Fig. S4. Among the PMF results, those for HP-WSOM, HULIS, and WISOM were selected for further data processing and analysis. Both four-factor and five-factor PMF solutions were tested, and each provided reasonable interpretations of the AMS spectra. To better capture the structural characteristics of the OA fractions, mainly a five-factor solution was used for the analysis in this study. The raw PMF-reconstructed OA signals for WISOM, HULIS, and HP-WSOM were $97.9 \pm 3.0\,\%$, $99.9 \pm 0.7\,\%$, and $91.3 \pm 6.3\,\%$ of the corresponding measured signals, respectively (mean $\pm$ SD). The atmospheric concentrations of OA masses associated with the PMF factors were derived from the concentrations of OA fractions with the approximation that the relative contribution of each factor to a given OA fraction is represented by the relative abundance of that factor among the five factors.

3 Results and discussion

3.1 Chemical structural characteristics of OA fractions

3.1.1 Composition and abundance of OA fractions

The average HR–AMS spectra of the three extracted fractions are shown in Fig. 1a. C_xH_y fragments representing hydrocarbon structures contributed as much as 63.7 % of the WISOM. As the polarity increases in the order of WISOM, HULIS, and HP-WSOM, the contribution of C_xH_y decreases, whereas that of $C_xH_yO_1$ and $C_xH_yO_{>1}$ (representing mono- and multioxygenated organic fragments, respectively) increase. The distributions of the fragment ion groups of the three fractions were generally similar to those of urban aerosols from our previous study (Zhou et al., 2021): $C_xH_yO_1$ dominated in HP-WSOM; C_xH_y and $C_xH_yO_1$ were comparable in HULIS; and C_xH_y was most abundant in WISOM. The O/C and H/C ratios and the OM/OC mass ratio for WISOM, HULIS, and HP-WSOM are shown in Fig. 1b. As the polarity increases in the order of WISOM, HULIS, and HP-WSOM, both the O/C and OM/OC ratios increase accordingly. HP-WSOM has the broadest range of O/C, H/C, and OM/OC values among the three fractions. The relative standard deviation of the O/C for HP-WSOM (24.4 %) was also greater than that for HULIS (9.3 %) and WISOM (16.1 %), likely reflecting greater chemical diversity or variability of HP-WSOM across different samples.

The seasonal variations in WISOM, HULIS, and HP-WSOM and the proportions of their averages are presented in Fig. 2. The average and standard deviation of the total OA, calculated as the sum of the three fractions, was $1.24 \pm 0.75\,\mu g\,m^{-3}$. With the exception of the two specific periods P1 (6 to 13 October) and P2 (9 to 16 March) with elevated total OA concentrations, OAs exhibited a clear seasonal pattern throughout the year. The relative contributions of the three fractions during P1 and P2 did not show particularly distinct changes compared with adjacent periods (Fig. 13a). The mean OA concentrations in summer, autumn, winter, and spring were 2.06, 0.94, 0.62, and $1.34\,\mu g\,m^{-3}$, respectively. The higher OA concentration in summer than in winter is consistent with the seasonal variations in OAs observed in long-term ACSM data (2012–2018) at SMEAR II (Heikkinen et al., 2020). Among the OA fractions, HP-WSOM, HULIS, and WISOM also peaked in summer (0.25 ± 0.11, 1.43 ± 0.64, and $0.39 \pm 0.17\,\mu g\,m^{-3}$, re-

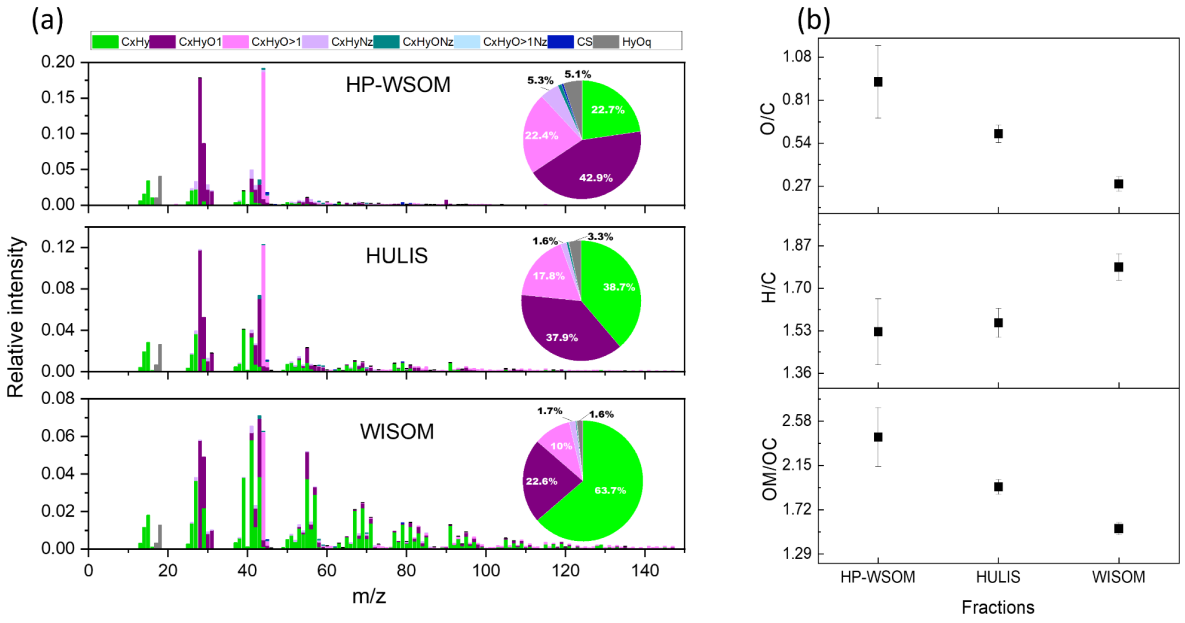

Figure 1. **(a)** Averages of the normalized HR–AMS spectra for HP-WSOM, HULIS, and WISOM with pie charts showing the averages of the fractional contributions of fragment ion groups. Different fragment groups are represented by different colors in the stacked bars. **(b)** O/C and H/C ratios and OM/OC mass ratios of HP-WSOM, HULIS, and WISOM.

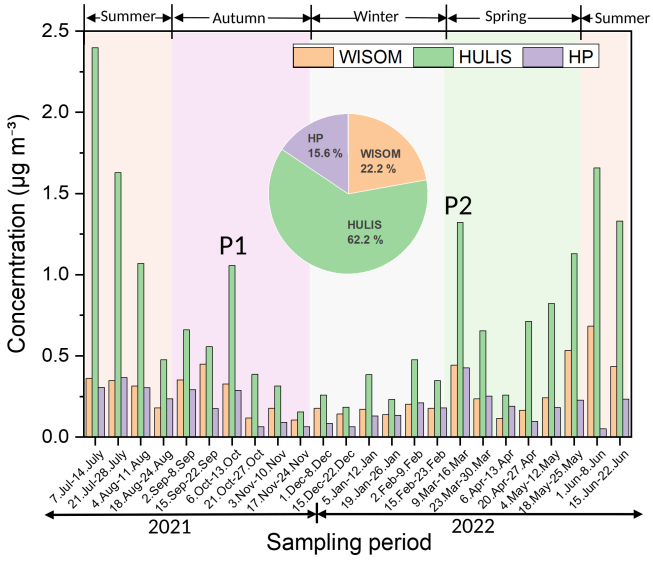

Figure 2. Seasonal variations in HP-WSOM, HULIS, and WISOM measured by HR–AMS, with the fractional contributions of their averages shown in the pie chart.

spectively) and reached their minima in winter (0.13 ± 0.06, 0.31 ± 0.11, and $0.17 \pm 0.02\,\mu g\,m^{-3}$, respectively), which is consistent with the trend of total OAs.

3.1.2 OA source regions during P1 and P2 events

To identify the potential source regions during the two events with elevated HULIS concentrations (P1 and P2), a PSCF analysis was performed using the 75th percentile of the particle volume concentration in the 100–1000 nm size range from the DMPS measurements. The calculated areas that were frequently traversed by the air masses that arrived at the study site during the high-concentration events are shown in Fig. 3.

In general, air masses passed over Scandinavia and other parts of Europe, and their passage over the North Atlantic Ocean and the Arctic Ocean was also evident. The potential source regions for the accumulation mode particles during P1 were located mainly southwest of the sampling site, the area covering southern Scandinavia and extending to the Kattegat region (northern Denmark and southwestern Sweden) (Fig. 3a). Significant anthropogenic OA precursor emissions in the Kattegat region, as inferred from large NO_x and non-methane volatile organic compound emissions there (Kuenen et al., 2022) may have contributed to the event, although the contribution from further long-range transport that was not detected in the PSCF analysis is not ruled out. Furthermore, Fig. 3a indicates additional contributions from the southeast, particularly Eastern Europe. The potential source regions for P2 were located mainly in the southeast, particularly western Russia, and also the Kattegat region. These spatial patterns are consistent with the findings of Riuttanen et al. (2013) who reported that clean air masses from the northwest were favorable for new particle formation, whereas air masses from the

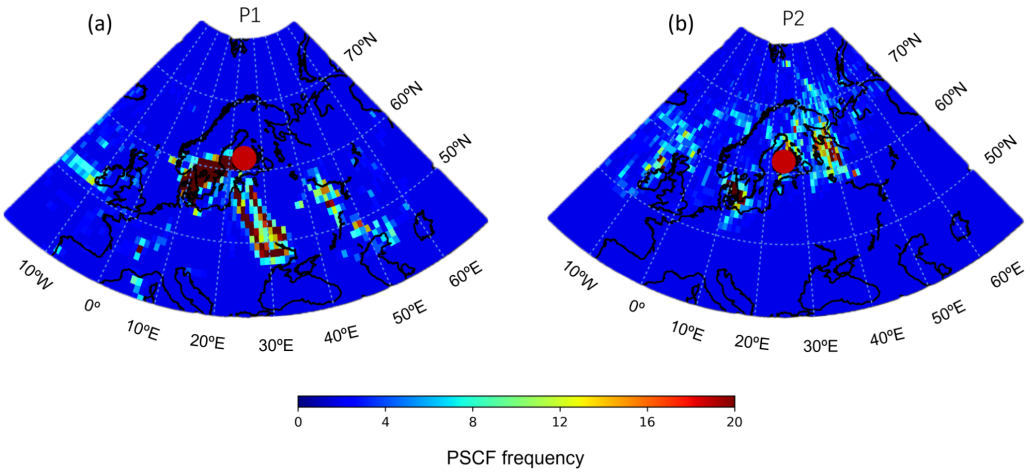

Figure 3. Potential source contribution function (PSCF) maps based on the 75th percentile of the DMPS-derived particle volume concentrations in the 100–1000 nm range. **(a)** P1 (6–13 October 2021). **(b)** P2 (9–16 March 2022).

southeast were typically associated with combustion-related accumulation mode particles, on the basis of a long-term backward trajectory analysis from 1996 to 2008. In line with this interpretation, the contributions observed in this study may reflect the influence of combustion-related emissions from industrialized and urban regions south and southeast of Hyytiälä (Riuttanen et al., 2013). However, these PSCF hotspots should be interpreted as transport-related potential source regions rather than exact emission locations. The backward trajectory analysis (Fig. S8) reveals the possibility of long-range transport for P1, whereas P2 is characterized by circulation patterns over the estimated source regions depicted in Fig. 3b, which are more conducive to the accumulation of pollutants. This may partly contribute to the higher OA concentration during P2 than during P1.

3.2 PMF-derived OA types

3.2.1 Overview of source apportionment

Different apportionment techniques have been applied to deconvolve organic matter (OM) at the SMEAR II station into various sources, as summarized in Table 1 (Raatikainen et al., 2010; Yttri et al., 2011; Finessi et al., 2012; Crippa et al., 2014; Äijälä et al., 2017, 2019; Corrigan et al., 2013; Vogel et al., 2013; Jiang et al., 2019; Kortelainen et al., 2017; Zhang et al., 2024; Heikkinen et al., 2021). Commonly identified factors include semivolatile oxygenated organic aerosol (SVOOA), low-volatile oxygenated organic aerosol (LVOOA), biomass burning organic aerosol (BBOA), and hydrocarbon-like organic aerosol (HOA) factors. A previous study performed source apportionment of submicron aerosol particles in Hyytiälä, Finland, during July and August 2010 by using aerosol mass spectrometry and Fourier transform infrared spectroscopy (FT-IR). While the study identified four major components – biomass burning, biogenic sources, and two fossil fuel-related factors (Corrigan et al., 2013) – it highlighted a high similarity between BSOA and BBOA AMS spectra, indicating the need for methods to better differentiate them. In this study, by employing HR–AMS to analyze specific fragment ions at high resolution, we aim to extract compound type information that enables a more robust distinction between these two aerosol types. Notably, since an offline extraction method was applied, the same PMF factor across different fractions should represent chemical structural characteristics in different sets of chemical species. As the focus of this work is on key chemical structural characteristics rather than on strict source attribution, we hereafter refer to them as BBOA-like and BSOA-like factors.

3.2.2 PMF results

The potential sources of WISOM, HULIS, and HP-WSOM were investigated by applying PMF analysis to their HR-AMS mass spectra, whereas WSOM was mainly used for methodological validation and was not included in the interpretation of the source apportionment results. PMF solutions with both the four factor and five factor solutions were considered to provide reasonable source interpretations, as described in Text S3. Whereas the four-factor solution consisted of more-oxidized oxygenated organic aerosol (MO-OOA), BBOA-like factor, BSOA-like factor, and HOA, the five-factor solution further separated an additional combustion-related organic aerosol (CROA) factor characterized by distinct aromatic structure. The five factor solution was used for further analysis in this study.

The time series and annual average contributions of the PMF factors are shown in Fig. 4. The factor with the lowest O/C ratio and the highest H/C ratio was associated with HOA, which were identified as the dominant component in WISOM, contributing 63 % of WISOM on average. MO-OOA in the present study should roughly corresponds to

Table 1. Summary of source apportionment studies at the Hyytiälä forest station.

Reference	Dataset	OA factors/types
Raatikainen et al. (2010)	Q-AMS	OOA1, OOA2
Yttri et al. (2011)	Thermal optical OC/EC, radiocarbon (^{14}C), HPLC–ESI–HRTOF-MS, GC	BSOA, BPAP, Fossil fuel, biomass burning
Finessi et al. (2012)	Q-AMS, ToF-AMS, NMR	AMS: OOA1, OOA2 NMR: HULIS-containing, amines, terpene SOA-like
Crippa et al. (2014)	AMS	HOA, BBOA, SVOOA, LVOOA
Äijälä et al. (2017)	C-ToF-AMS	HOA, COA, SVOOA, LVOOA, sawmill SOA
Äijälä et al. (2019)	ToF-AMS, C-ToF-AMS	Ammonium sulfate, ammonium nitrate, SVOOA, LVOOA, BBOA, nitrate-containing type, HOA
Corrigan et al. (2013)	FT-IR, C-ToF-AMS	BSOA, BBOA, FFC1, FFC2
Vogel et al. (2013)	AMS	OOA1, OOA2
Jiang et al. (2019)	ACSM, AMS	HOA, BBOA, OOA
Kortelainen et al. (2017)	HR–AMS	SV-OOA, LV-OOA and NO-factor
Zhang et al. (2024)	LToF-AMS	Inorganic, OOA, HOA, BBOA, Kola pollution
Heikkinen et al. (2021)	ACSM	SV-OOA, LV-OOA and POA
This study	HR–AMS	MO-OOA, BBOA-like, BSOA-like, CROA, HOA

LVOOA in some earlier studies because it showed a high O/C ratio and strong oxygenated fragment ion signals. The BSOA-like factor may be more closely related to SVOOA in earlier studies because it was less oxidized than MO-OOA and likely represented relatively fresh SOA (Ng et al., 2010). The terminology adopted here emphasizes oxidation level rather than volatility due to the lack of volatility measurements and because O : C, or the degree of oxygenation, does not necessarily provide a direct measure of volatility (Zhang et al., 2011). MO-OOA exhibited the highest O/C ratio of 1.18, were the dominant component in HP-WSOM, accounting for 73.7 % of HP-WSOM on average. These findings are consistent with our previous study, where HOA was also reported as a major contributor to WISOM (77 %), and MO-OOA dominated the HP-WSOM fraction (96 %) (Zhou et al., 2021). The source identification of the remaining three factors is discussed in detail in the following sections.

3.2.3 BSOA-like tracers and related chemical structural characteristics

The identification of the BSOA-like factor is partly based on its characteristic seasonal pattern. During summer, BSOA-like factor accounted for up to 68.2 % of HULIS, which is consistent with the enhanced BVOC emissions under higher temperatures and stronger solar radiation in summer than in the other seasons. The identification of the BSOA-like factor is further supported by the seasonal pattern closely resembling that of temperature and solar radiation (Fig. 5a). As shown in Fig. 6, BSOA-like factor was strongly correlated with temperature ($r = 0.83$), solar radiation ($r = 0.73$), and MBO (a biogenic volatile organic compound primarily emitted by coniferous trees such as pines; $r = 0.70$), whereas the correlations with the other PMF factors were notably weaker. These correlations further support the biogenic secondary formation of the OA mass corresponding to the BSOA-like factor. We observed that when OAs increased during P1 and P2 events, the concentrations of the BSOA-like factor also increased (Fig. 4b). The possible explanations include the transport of BSOA from the upwind region and the enhancing effect of anthropogenic pollution on BSOA (Nguyen et al., 2014).

To further investigate the chemical structural characteristics of the BSOA-like factor, we analyzed several fragment ions (Fig. 5b) associated with the gaseous precursors (BVOCs). We selected $C_5H_7^+$ (m/z 67), $C_6H_9^+$ (m/z 81), and $C_7H_7^+$ (m/z 91) as representative medium-mass hydrocarbon-type markers since all have been reported as fragmentation ions characteristic of BSOA in several studies (Boyd et al., 2015; Bahreini et al., 2005; Kiendler-Scharr et al., 2009; Robinson et al., 2011). Although hydrocarbon-type fragment ions were detected at relatively high levels, they exhibited limited source specificity. Therefore, we also considered the higher mass but less abundant ions $C_7H_9O_3^+$ and $C_9H_{13}O_4^+$. The fragment ion $C_7H_9O_3^+$ (m/z 141) has been proposed as a signature for

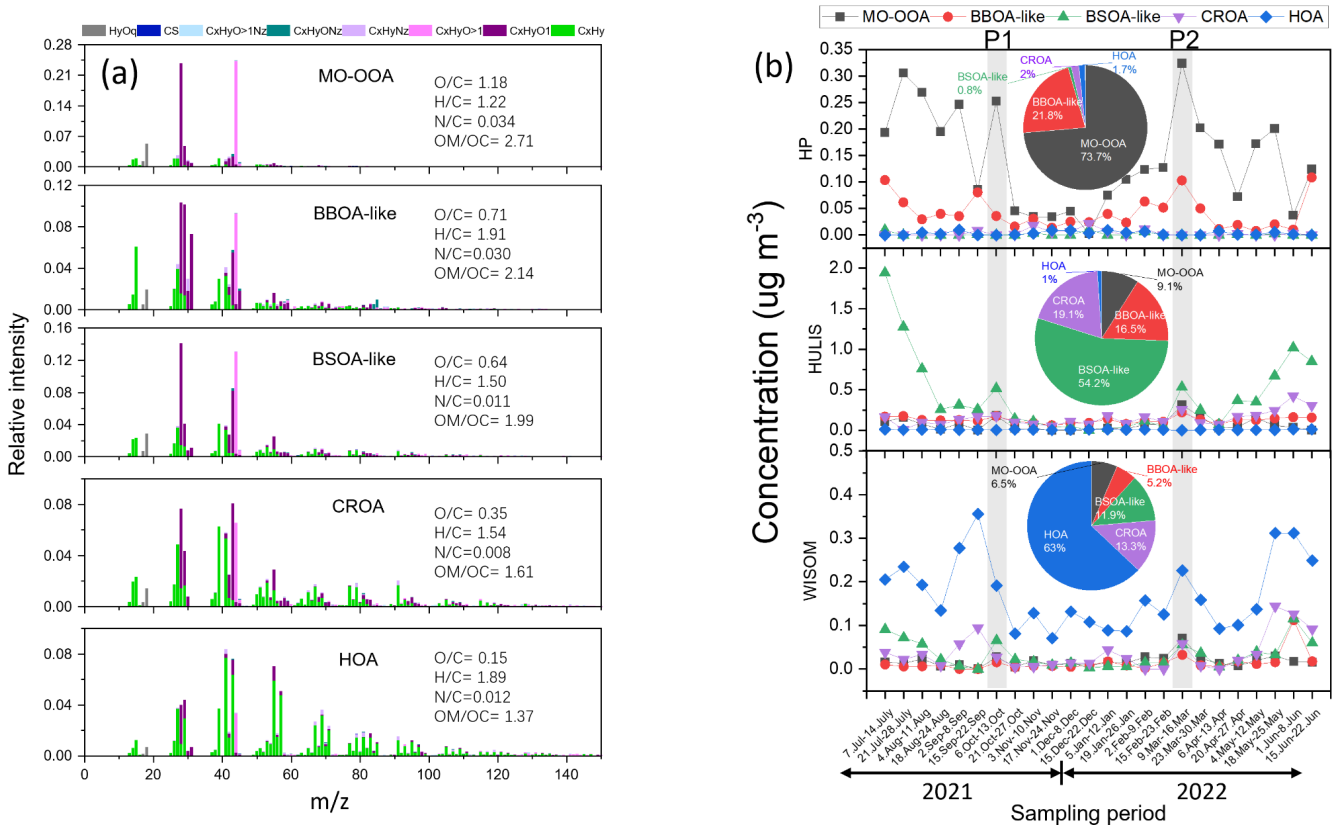

Figure 4. **(a)** HR–AMS spectra of the five PMF-derived factors and their elemental analysis data. **(b)** Time series of the concentrations of MO-OOA, BBOA-like, BSOA-like, CROA, and HOA in HP-WSOM, HULIS, and WISOM and the proportions of the mean concentrations.

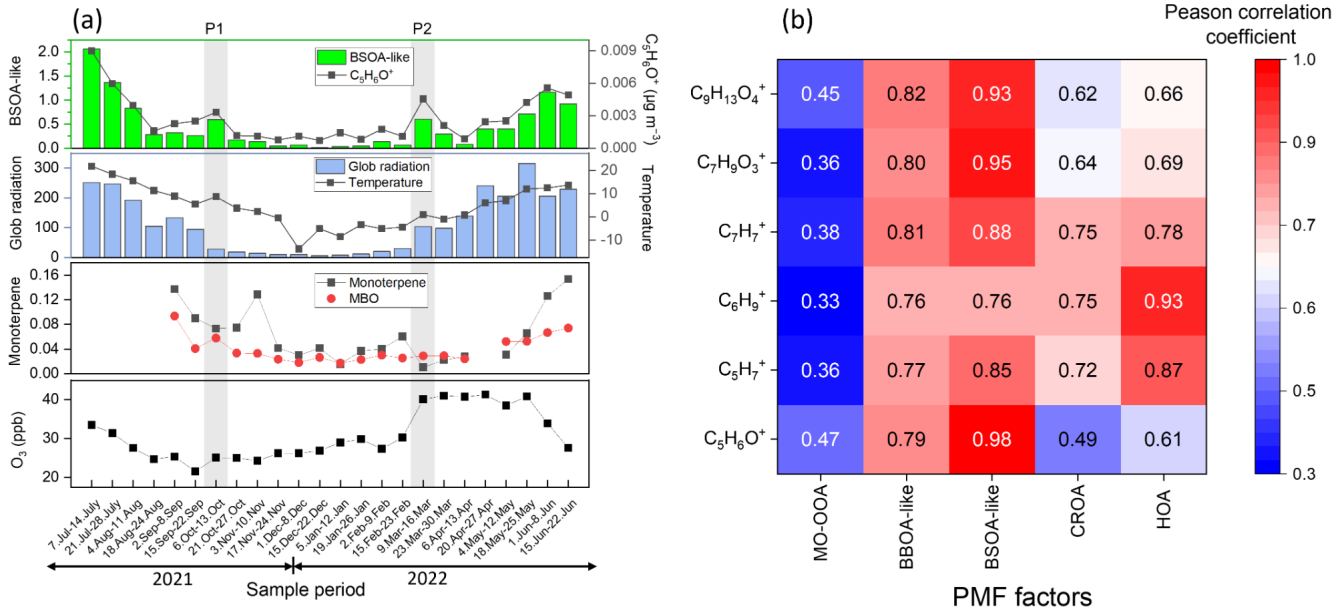

Figure 5. **(a)** Time series of BSOA-like factor and $C_5H_6O^+$ concentration, along with those of global radiation, temperature, monoterpenes, MBO, and O_3 (data from SmartSMEAR: https://smear.avaa.csc.fi/, last access: 5 February 2025). **(b)** Correlation matrix illustrating the relationships between PMF-derived factors and the sum of characteristic fragment ions from HP-WSOM, HULIS, and WISOM.

3-methyl-1,2,3-butanetricarboxylic acid (MBTCA), a tracer compound indicative of terpene-derived SOAs (Kostenidou et al., 2018). $C_9H_{13}O_4^+$ (m/z 185) corresponds to the deprotonated form of $C_9H_{14}O_4$ terpenoic acids with a molecular weight of 186, such as cis-pinic acid (Yasmeen et al., 2011). $C_5H_6O^+$ (m/z 82) is a fragment ion widely recognized in field studies as a tracer for IEPOX-derived SOAs formed from isoprene oxidation under low-NO conditions, but it can also be substantially influenced by monoterpene-derived SOAs (Hu et al., 2015; Robinson et al., 2011).

These ions were strongly correlated with the BSOA-like factor, jointly supporting the identification of this factor, as presented in Fig. 5b. In this study, $C_5H_6O^+$ exhibited a very strong correlation coefficient exclusively with the BSOA-like factor ($r = 0.98$). The seasonal variation of $C_5H_6O^+$ concentration is highly consistent with that of the BSOA-like factor (Fig. 5a). Although $C_5H_6O^+$ is generally regarded as a fragment ion that is indicative of isoprene oxidation, monoterpene-derived SOAs can also enhance its signal, as mentioned above (Hu et al., 2015). In addition, while monoterpenes dominate the mixing ratios during summer in Hyytiälä, the presence of isoprene is also evident (Hakola et al., 2012; Fischer et al., 2021). Therefore, both isoprene- and monoterpene-derived SOAs may be associated with the observed $C_5H_6O^+$ signal in this study. Despite its strong correlation with the BSOA-like factor and its relative abundance falling within the range reported for monoterpene-derived SOA by Hu et al. (2015), $C_5H_6O^+$ should be interpreted with caution as a standalone tracer, because its relative abundance was high in in the mass spectrum of CROA factor in addition to that of BBOA-like factor (Table S6). The medium-mass hydrocarbon-type fragment ions $C_5H_7^+$ (m/z 67), $C_6H_9^+$ (m/z 81), and $C_7H_7^+$ (m/z 91) also exhibited high correlations with the BSOA-like factor ($r = 0.85$, 0.76, and 0.88, respectively). However, their specificity as tracers of BSOA was limited. For example, HOA showed even stronger correlations with $C_5H_7^+$ and $C_6H_9^+$ than BSOA-like factor did, which is not unexpected because these two are hydrocarbon fragment ions and showed their largest contributions from HOA among the factors (Table S7). Given that BVOCs are abundant in hydrocarbons, HOA is presumably influenced by freshly formed biogenic aerosols in addition to generally recognized fossil fuel combustion emissions. This is supported by the strong correlation of HOA with MBO ($r = 0.69$) and by the finding that HOA showed the second-strongest correlations among those involving temperature ($r = 0.55$) and among those involving solar radiation ($r = 0.55$). Considering the ubiquitous occurrence of hydrocarbons across different sources, these medium-mass hydrocarbon-type ions are unlikely to serve as BSOA tracers by themselves, but they could provide supportive evidence when used in combination with other marker ions. The abundance of higher-mass ions $C_7H_9O_3^+$ and $C_9H_{13}O_4^+$ was 1–2 orders of magnitude lower than that of the medium-mass ions mentioned, presumably because of extensive fragmentation under ~ 70 eV electron ionization (EI). Nevertheless, they were detected by the spectral peak fittings (Fig. S10) and exhibited notable source specificity and correlated strongly and exclusively with the BSOA-like factor (r: 0.95 and 0.93, respectively). Although their relative abundances are high in CROA factor as well as in BSOA-like factor (Table S6), $C_7H_9O_3^+$ and $C_9H_{13}O_4^+$ could serve as auxiliary characteristic ions of BSOA-like factor in future EI-based mass spectrometric studies of OAs, together with other supporting evidence.

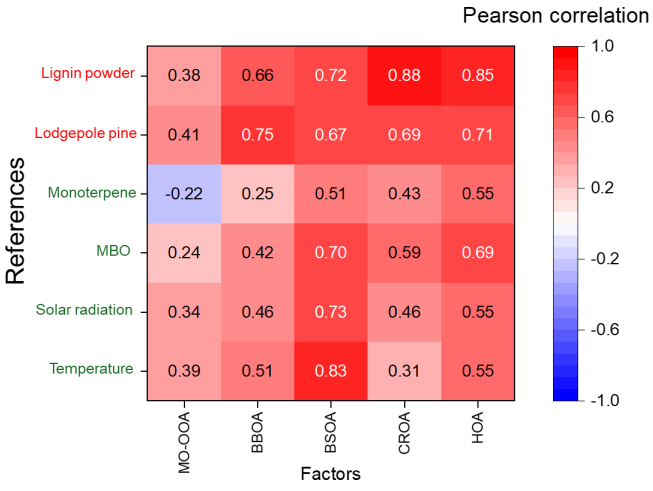

Figure 6. Pearson correlation coefficients between PMF-resolved OA factors and six selected references. The references include two meteorological parameters (temperature and solar radiation, data from SmartSMEAR) and two BVOCs (monoterpene and MBO, also from SmartSMEAR), for which correlations are based on temporal variations, as well as two biomass burning HR–AMS spectra for which correlations are based on mass spectral similarity (from the AMS Spectral Database, URL: http://cires.colorado.edu/jimenez-group/AMSsd/, last access: 16 April 2025) (Ulbrich et al., 2009b).

3.2.4 BBOA-like tracers and related chemical structural characteristics

To confirm the identification of the BBOA-like factor, we compared the UMR spectra of five PMF factors with the AMS spectrum of aerosols from chamber-burned lodgepole pine (needles and sticks) from the AMS spectral database (Ulbrich et al., 2009b) (Fig. S6a). As a coniferous species similar to Scots pine, one of the main forest-forming tree species in Fennoscandia (Heikkinen et al., 2021; Kuuluvainen and Aakala, 2011), lodgepole pine provides a relevant reference for comparison. The BBOA-like factor exhibited the highest correlation coefficient ($r = 0.75$) among the five PMF factors (Fig. 6), supporting its association with BBOA.

The time series of non-sea-salt (nss)-SO_4^{2-} and nss-K^+ from ion chromatography are shown in Fig. 7. Nss-K^+ and nss-SO_4^{2-} were calculated by subtracting the contributions of sea-salts by assuming that Na^+ is totally from seawa-

ter (Kunwar and Kawamura, 2014; Seinfeld and Pandis, 2016). The nss-K^+ concentration is widely used as an indicator of the influence of biomass burning, although it could also be affected by other sources, such as agricultural activities and soil resuspension (Andreae, 1983; Zhang et al., 2010). Despite a weak correlation with the BBOA-like factor ($r = 0.30$), nss-K^+ exhibited a pronounced increase during both P1 and P2, whereas other cations did not show similar patterns, suggesting episodic biomass-burning influences. The sources of nss-SO_4^{2-} are complex and generally represent secondary inorganic aerosols generated from anthropogenic sulfur dioxide, marine biogenic precursors, volcanic emissions and so forth (Seinfeld and Pandis, 2016). The correlation of nss-SO_4^{2-} with the BBOA-like factor was modest ($r = 0.45$), and nss-SO_4^{2-} did not show a clear increase during P2 while showed an increase during P1. The results indicate that the BBOA-like factor was not coupled to sulfate sources such as fossil-fuel combustion, as expected.

As explained in the introduction section, BBOA generally contain NOC fragment ions from both CHN and CHON family compounds, whereas BSOA predominantly consist of CHON family compounds formed through the oxidation and nitration of BVOCs (Laskin et al., 2014; Laskin et al., 2009). On the basis of this distinction, we consider that CHN family ions can serve as tracers for differentiating BBOA from BSOA. As shown in Fig. 7, the concentration of the BBOA-like factor exhibits a variation pattern closely aligned with that of the CHN family, with a high correlation coefficient ($r = 0.85$).

To further investigate the characteristics of the CHN family compounds, we listed all CHN family ions quantified and calculated their corresponding annual average concentrations, as shown in Fig. 8a. The distribution of the CHN family ions among the three OA fractions revealed the high water solubility of the compounds from which they originated. An average of 76.3 % of the total CHN family ions were from water-soluble compounds, and smaller ions tended to originate more from water-soluble compounds. Among the CHN family ions, CHN^+, CH_4N^+, and $C_2H_3N^+$ were the most abundant. Previous chamber and field studies have reported that CH_4N^+ can serve as a tracer ion for amines (Ge et al., 2024) and that $C_nH_{2n-1}N^+$ and $C_nH_{2n-2}N^+$ are likely associated with nitriles (Ge et al., 2024; McLafferty and Turecek, 1993). Although CHN family ions may also originate from sources other than BBOA, such as primary biological aerosol particles (PBAPs, including bacteria, fungal spores, etc.) and biogenic amine partitioning, their contributions are expected to be limited in the present study. This is because the analyzed samples were $PM_{0.95}$, whereas PBAPs are generally enriched in the coarse particle size range. In addition, previous measurements at SMEAR II showed that gas-phase organic amines were present at very low concentrations, although they can be important for new particle formation (Hemmilä et al., 2018; Sipilä et al., 2015). Therefore, the presence of amines and nitriles supports the proposed formation pathway of CHN family compounds in BBOA, as outlined in the introduction: high-temperature biomass combustion facilitates the release of ammonia and amines, followed by reactions with carboxylic acids to form alkyl amides and subsequent dehydration to produce alkyl nitriles.

This study also considers the performance of the tracer ion from levoglucosan (and possibly from similar compounds including its isomers), $C_2H_4O_2^+$ (unit mass m/z 60). Previous studies conducted at Hyytiälä suggested that m/z 60 is difficult to observe at this site because of degradation during long-range transport (Corrigan et al., 2013; Zhang et al., 2024). As shown in Fig. 1a, the relative abundance of m/z 60 was very low, accounting for only approximately 0.23 %, 0.086 %, and 0.094 % of the total signal in HP-WSOM, HULIS, and WISOM, respectively. The presence of BBOA-like signals in HP-WSOM may reflect aged or secondary biomass-burning-related products, even though levoglucosan may have been depleted. The background level of m/z 60 for SOA-dominated ambient OA has been reported to be $0.3\,\% \pm 0.06\,\%$ (Cubison et al., 2011). The relative abundances of m/z 60 in the three fractions were all lower than or close to this background level. This is likely because levoglucosan generally has a short atmospheric lifetime. Our previous field study suggests that a considerable fraction of levoglucosan remained detectable after 4–5 d of wintertime transport, whereas substantial depletion occurred during summer transport (Mochida et al., 2010). Further, laboratory experiments estimated a particle-phase lifetime of 0.7–2.2 d under typical summertime OH exposure, while a global model estimated a mean atmospheric lifetime of 1.8 d (Li et al., 2021; Hennigan et al., 2010). In addition to degradation during atmospheric transport, the one-week filter sampling used in this study may further contribute to the loss of levoglucosan and its related ions.

CHN-family ions in AMS spectra represent a broader group of nitrogen-containing organic fragment ions. Therefore, even when individual CHN-containing molecular species undergo chemical transformation, the resulting products may still remain within the broader CHN-containing chemical class (Li et al., 2024). Conversely, although levoglucosan is not the only contributor to the m/z 60 ion signal (Lee et al., 2010), if this signal originates primarily from the chemical structures of anhydrosugars, atmospheric degradation of these structures would be closely associated with the loss of the m/z 60 signal (Hennigan et al., 2010). For CHN-containing compounds, molecular-level characterization of laboratory-generated BBOA showed that, after approximately 7 d of atmospheric-equivalent aging, the overall CHN signal remained at approximately 91 %–112 % of the corresponding fresh-BBOA values (Li et al., 2024). These results indicate that the signals from broader CHN-containing compounds may be more resistant to aging, despite the transformation of individual compounds. However, we cannot exclude the possibility that the secondary forma-

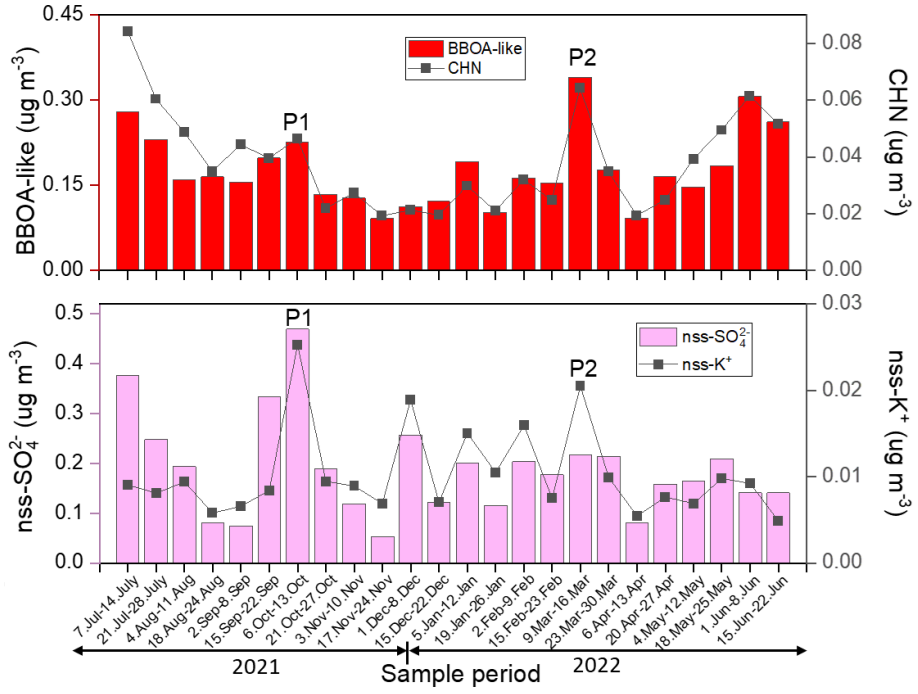

Figure 7. Time series of BBOA-like factor, CHN family ions, nss-SO_4^{2-} and nss-K^+.

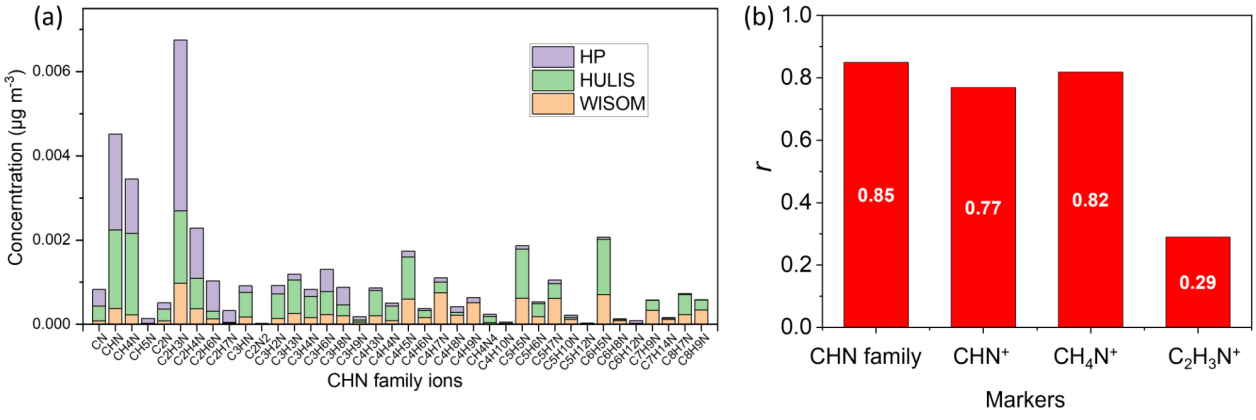

Figure 8. **(a)** Annual average concentrations of the OA mass detected as different CHN family ions in HP-WSOM, HULIS, and WISOM. **(b)** Correlation coefficients of the time series of BBOA-like factor with the series of total CHN family ions and individual ions (CHN^+, CH_4N^+, and $C_2H_3N^+$).

tion of nitrogen-containing compounds during atmospheric transport introduces uncertainty into the source apportionment.

3.2.5 Comparison of BBOA-like, CROA and BSOA-like structures

The association to sources for BBOA-like, CROA, and BSOA-like factors, which did not show distinct O/C characteristics like MO-OOA were further examined. Because EC is mainly produced by incomplete combustion processes, including fossil fuel combustion, biomass burning, and coal combustion, the EC/OC ratio is commonly used as an auxiliary indicator of combustion-related aerosol influence (Wang et al., 2018). As shown in Fig. 9, the seasonal variations of the relative contributions of the BBOA-like and CROA factors were generally well correlated with variations in the EC/OC ratio, with relatively high contributions in winter. These seasonal patterns support that these two factors were influenced by combustion-related sources, being consistent with the discussion based on their mass spectral characteristics. In contrast, the relative contribution of the BSOA-like factor exhibited an opposite seasonality to the EC/OC ratio, indicating its weak association with combustion emissions.

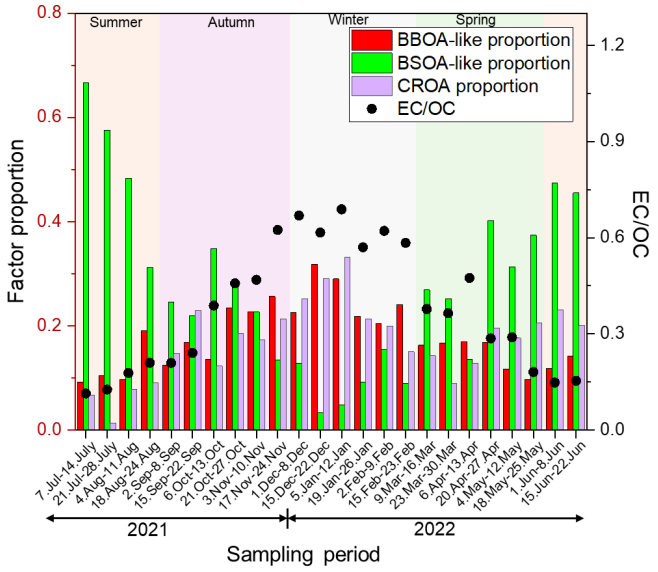

Figure 9. Seasonal variations in the relative contributions of BBOA-like, BSOA-like, and CROA factors, together with the EC/OC ratio.

Although both the CROA and BBOA-like factors are considered to be related to combustion sources, the structural differences between the CROA and BBOA-like factors are clear. The mass spectra of these two factors in Fig. 10 show that CROA are characterized by aromatic fragment ions, such as $C_6H_5^+$ (m/z 77), $C_6H_7^+$ (m/z 79), and $C_7H_7^+$ (m/z 91). One possible explanation is that the CROA factor is related to aged OAs originating from fossil fuel emissions. Whereas a PMF factor associated with fresh OAs from fossil fuel combustion, as a type of POA, typically results in a low O/C ratio, for example, 0.14 in central eastern China (Hu et al., 2017) and 0.17 in Beijing (Zhou et al., 2021), the CROA factor in this study shows a higher O/C ratio of 0.35. Moreover, OAs from fossil fuel are expected to be distributed primarily in WISOM (Zhou et al., 2021), whereas in our case, 79.5 % (annual average) of the CROA mass was found in the HULIS fraction, suggesting a higher water solubility, which is consistent with the higher degree of oxidation.

Another explanation is that the CROA factor originated from the combustion of aged biomass materials. This finding is supported by a recent study (Ma et al., 2024), which proposed that the composition of OAs originating from biomass burning emissions can be classified into two types: OAs from the combustion of fresh biomass and OAs from the combustion of aged biomass. Fresh biomass, such as vegetation burned in forest fires, is typically rich in nutrients, including lipids and proteins. As discussed in Sect. 3.2.4, our BBOA-like factor is characterized by CHN family ions, including CHN^+ (m/z 27), CH_4N^+ (m/z 30), and $C_2H_3N^+$ (m/z 41), which are indicative of the combustion of protein-rich fresh biomass. In contrast, aged biomass, including postharvest straw, fallen leaves, and deadwood, is generally nutrient poor, with abundant lignin (Ma et al., 2024). The pyrolysis or combustion of lignin releases large amounts of aromatic compounds (Simoneit, 2002), as evidenced by aromatic peaks in the reference spectrum of lignin powder retrieved from the AMS spectral database (Ulbrich et al., 2009b) (Fig. S6b). Among the five PMF factors, the CROA factor exhibits the highest spectral similarity with lignin combustion ($r = 0.88$), exceeding those of the MO-OOA ($r = 0.38$), BBOA-like ($r = 0.66$), BSOA-like ($r = 0.72$), and HOA ($r = 0.85$) factors, supporting its association with lignin-rich sources. Furthermore, as shown in Fig. 4a, the N/C ratio of the BBOA-like factor (0.03) was substantially higher than that of the CROA factor (0.008). These findings suggest that BBOA-like compounds are closely associated with the combustion of fresh biomass, whereas the aromatic character of CROA is linked to fossil fuel-derived OAs and/or the burning of aged biomass.

The N/C ratio of BSOA-like factor (0.011) lies between the ratios of BBOA-like and CROA factors, which may be attributed to the formation of oxygen- and nitrogen-containing organic compounds (NOCs) via the oxidation and nitration of biogenic VOCs (BVOCs). In addition, the mass spectral profile of BSOA-like factor also contains signals of aromatic-like fragment ions such as $C_6H_5^+$ (m/z 77), $C_6H_7^+$ (m/z 79), and $C_7H_7^+$ (m/z 91), although their intensities are much weaker than those of CROA. Similar features have been observed in the HR–AMS spectra from chamber experiments of SOAs generated from α-pinene ozonolysis and oxidation under high-NO_x conditions (Chhabra et al., 2011; Chhabra et al., 2010), indicating that the presence of aromatic-like signals (potentially derived from nonaromatic precursors) in BSOA-like factor is not unexpected. In the higher m/z range (100–150), the differences between BSOA-like and CROA factors become more evident: CROA is dominated by C_xH_y family ions, contributing 41.3 % of the total signal compared with 24.1 % in BSOA-like factor, whereas BSOA-like factor is enriched in $C_xH_yO_{>1}$ ions, reaching 42.6 % compared with 24.9 % in CROA.

3.3 Application of PMF for fractionation-based offline AMS analysis

3.3.1 PMF factors

The seasonal variations in the relative contributions of the five PMF factors throughout the year are shown in Fig. 11. Among them, the BSOA-like factor was the only factor that exhibited a clear summertime maximum and wintertime minimum, with its mean seasonal contribution reaching 49 % in summer, indicating that BSOA-like factor were the dominant contributors to OAs during this period. In Hyytiälä, the average temperature for the respective filter sampling periods exceeded 20 °C only during the first sampling period (7–14 July), when the average temperature reached 21.8 °C

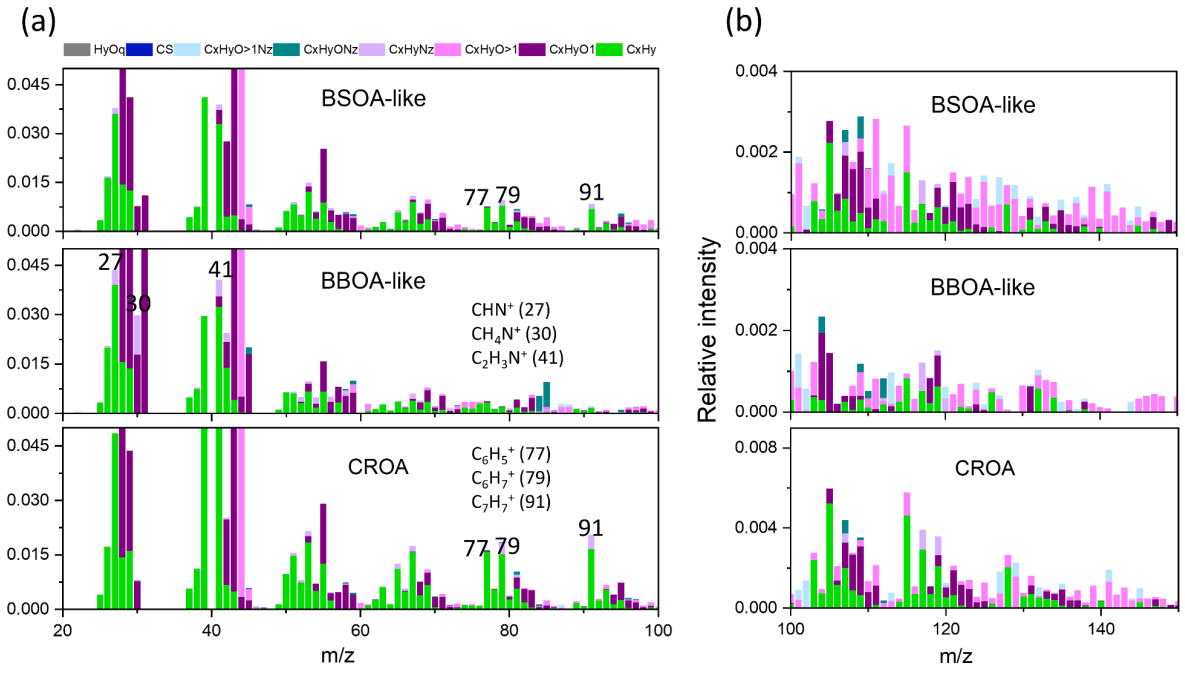

Figure 10. **(a)** Enlarged mass spectra of the BSOA-like, BBOA-like, and CROA factors with annotated characteristic fragment ions in the m/z range 20–100 (some prominent peaks are outside the vertical axis range; the full-scale spectra are shown in Fig. 4a). **(b)** Enlarged mass spectra of the BSOA-like, BBOA-like, and CROA factors in the m/z range of 100–150.

(Fig. 5a). During this period, BSOA-like factor accounted for 66.7 % of the total OAs, which was the highest among the studied periods.

In contrast to BSOA-like factor, BBOA-like factor and CROA factor exhibited opposite seasonal variation patterns, with peaks of seasonal average contributions of 25 % and 24 % in winter, respectively, and lower contributions of 12 % and 11 % during summer, respectively. In addition, the mass contributions of BBOA-like factor and CROA factor were correlated throughout the year ($r = 0.63$). On the basis of previous studies, the combustion-related aerosols observed at Hyytiälä are predominantly transferred by air masses from the southeast (Riuttanen et al., 2013).

HOA exhibited the greatest relative contributions in autumn and winter, both of which reached 22 % on average, likely reflecting increased fossil fuel consumption due to residential heating during cold months. In contrast, MO-OOA did not show a pronounced seasonal pattern; MO-OOA contribution peaked in spring and reached 27 % on average, which may be associated with enhanced photochemical activity due to long daylight hours and elevated levels of atmospheric oxidants such as ozone (Fig. 5a).

3.3.2 Solubility analysis with PMF factors

To gain further insight into the solubility characteristics of the PMF factors, the proportions of the water-insoluble fractions (f_{WISOM}) of the five PMF factors were calculated from their concentrations in the three OA fractions (Fig. 12). The majority of HOA was distributed in the WISOM fraction, with an annual average of 92.4 ± 4.8 % (mean $\pm$ SD), indicating consistently water-insoluble characteristics of the compounds associated with this factor. The f_{WISOM} of CROA was lower, with an annual average of 17.8 ± 15.2 %, and was generally higher than that of BBOA-like factor (7.0 ± 7.5 %). The difference is likely associated with the distinct structural characteristics of the two factors: BBOA-like factor is enriched in CHN family compounds, whose polar functional groups (e.g., amino group) should enhance hydrophilicity, whereas CROA shows stronger signals of aromatic structures, which should enhance hydrophobicity. The annual average water-insoluble fraction of MO-OOA was low (11.1 ± 9.8 %), consistent with its high oxygenation degree, which introduces polarity to molecules. It should be noted that part of the variability shown in Fig. 12 may arise from uncertainties in the PMF-derived fractional values, especially when the corresponding factor concentrations were very low.

The annual average f_{WISOM} of the BSOA-like factor was 10.8 ± 6.5 %, which also indicated water-soluble characteristics. Owing to the very low fraction of the BSOA-like factor in winter, large uncertainties may exist during this period. If the winter values are excluded, the WISOM fraction was 8.4 % on average. Previous chamber and field studies have demonstrated that BSOA is generally mostly water soluble. For instance, the soluble fraction of isoprene-derived SOAs has been reported to exceed 80 % (Xu et al., 2017), whereas

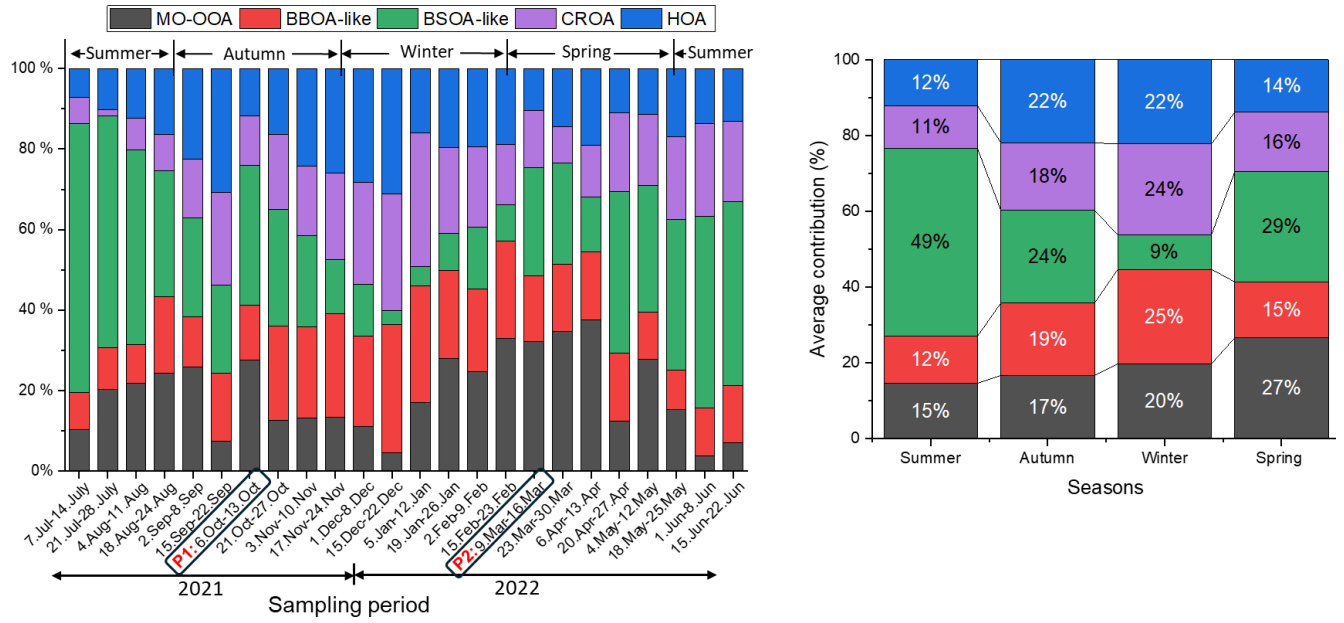

Figure 11. Relative contributions of PMF factors to total OAs.

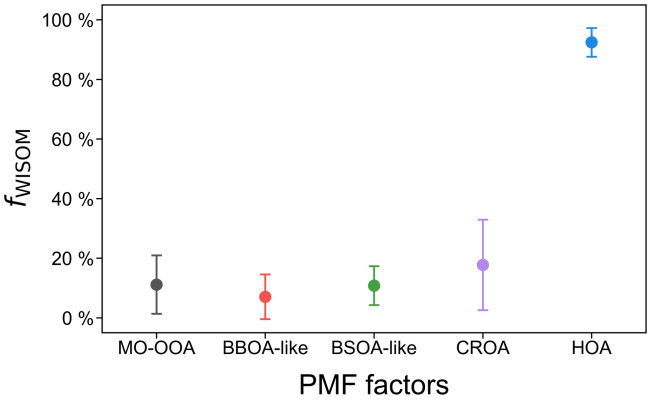

Figure 12. Proportions of the water-insoluble fractions of the five PMF factors. The markers and bars represent the mean and standard deviation, respectively.

that of limonene-derived SOAs generated in chamber experiments may exceed 95 % (Bateman et al., 2010). The results of the present study are in reasonable agreement with those of previous studies.

3.3.3 Polarity distribution analysis with PMF factors

The seasonal variations in the proportions of HP-WSOM, HULIS, and WISOM are presented in Fig. 13a. The seasonal variation patterns reveal that HULIS dominated in summer and made a lower contribution in winter. This seasonality is linked to the dominant PMF factors in each fraction (Figs. 4b and 11). The BSOA-like factor was the largest contributor to the intermediate-polarity HULIS fraction, accounting for 54.2 % on average, and this factor exhibited a clear summertime enhancement. The mean HULIS concentration increased by 1.1 $\mu g\,m^{-3}$ from winter to summer, of which 0.97 $\mu g\,m^{-3}$ (87.1 %) was accounted for by the increase in the BSOA-like factor. HP-WSOM and WISOM were dominated by MO-OOA and HOA (Fig. 4b), with mean contributions of 73.7 % and 63.0 %, respectively. The seasonal mean concentrations of HP-WSOM and WISOM increased by 0.12 and 0.22 $\mu g\,m^{-3}$ from winter to summer, respectively, with substantial increases of MO-OOA (0.11 $\mu g\,m^{-3}$) and HOA (0.11 $\mu g\,m^{-3}$). The other factors contributed only slightly to the changes from winter to summer (from −0.01 to 0.06 $\mu g\,m^{-3}$). Although HP-WSOM and WISOM and their dominant factors also increased in summer, the BSOA-related enhancement of HULIS was the primary driver of the winter-summer redistribution among the three fractions.

According to a previous study, HOA is strongly associated with fossil fuel emissions and is therefore the dominant contributor to WISOM across all seasons in urban environments (Zhou et al., 2021). However, as discussed in Sect. 3.2.3, we suggest that during summer in Hyytiälä, the HOA factor contributing to WISOM is not only associated with fossil fuel emissions, but also influenced by fresh biogenic aerosols. WISOM showed the greatest seasonal contribution in winter, reaching 30.4 %, followed by autumn (28.2 %), spring (22.1 %), and summer (19.8 %). Although this seasonal pattern may be primarily attributed to the wintertime decrease in the HULIS fraction, which is associated with the BSOA-like factor, the contribution of fossil fuel-derived aerosols in winter may also be a reason. The OC/EC ratios from the thermal/optical analysis exhibited a pronounced seasonal pattern, with the highest mean value of 6.72 in summer (Fig. S2b), in-

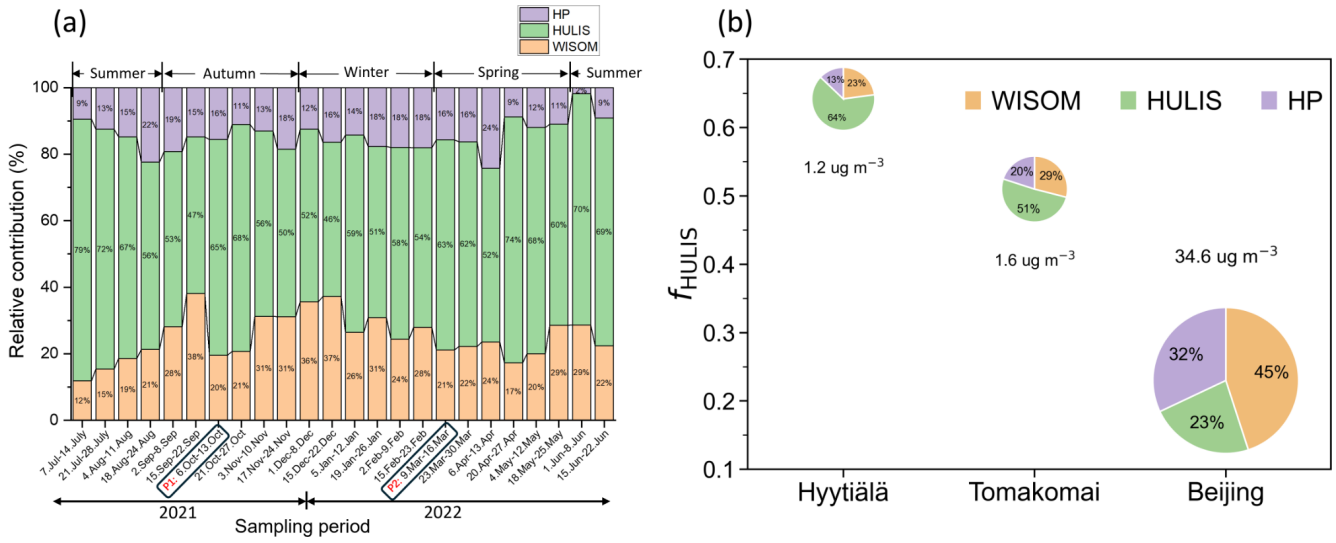

Figure 13. **(a)** Relative contributions of HP-WSOM, HULIS, and WISOM to total OAs. **(b)** Annual mean values of the proportions of HP-WSOM, HULIS, and WISOM with annual average OA concentrations at three sites in Hyytiälä, Tomakomai, and Beijing.

dicating a significant contribution of secondary OAs. In contrast, the lowest mean OC/EC value of 1.61 was observed in the winter. This finding indicates the enhanced influence of fossil fuel-derived aerosols, including EC, during winter and explains the increased WISOM fraction.

The pie charts in Fig. 13b show the annual mean proportions of HP-WSOM, HULIS, and WISOM at Hyytiälä (Finland) and two other sites: Tomakomai (Japan) and Beijing (China). The three sampling sites are considered to represent a gradient of anthropogenic influence: Hyytiälä in Finland is a boreal forest background site with minimal local emissions; the Tomakomai experimental forest (TOEF) in Hokkaido, Japan, is a cool-temperate forest site subject to regional and moderate anthropogenic influence; and Beijing, China, is a megacity strongly affected by fossil fuel combustion and other human activities. The OA concentrations at the three sites tended to increase with increasing degree of anthropogenic influence, with mean annual values of 1.2, 1.6, and 34.6 µg m^{-3} at Hyytiälä, Tomakomai, and Beijing, respectively. At the clean forest site of Hyytiälä, HULIS constituted the dominant fraction, accounting for 64 %, followed by WISOM (23 %) and HP-WSOM (13 %). A similar distribution but with a lower proportion of HULIS was reported for the forest site of Tomakomai, where HULIS accounted for 51 %, WISOM accounted for 29 %, and HP-WSOM accounted for 20 % (Afsana et al., 2022). The proportions of urban aerosols in Beijing markedly differed, with WISOM accounting for 45 %, followed by HP-WSOM (32 %) and HULIS (23 %) (Zhou et al., 2021). Source apportionment based on the PMF analysis in the present study can help explain this difference. In forest regions, particularly in summer, the BSOA-like factor contributes substantially to HULIS, whereas such a contribution is not expected in urban areas. In the case of WISOM, which is strongly associated with fossil fuel OAs, traffic emissions in densely populated urban areas should contribute heavily. As a result, forested regions, especially in summer, were dominated by HULIS, whereas WISOM accounted for the greatest fraction in urban areas.

4 Summary and conclusions

In this study, offline chemical structural characteristic analysis and PMF-based source apportionment of OAs in a boreal coniferous forest in Finland were performed. The samples were extracted into three fractions of varying polarities: HP-WSOM, HULIS, and WISOM. This study is based on sampling in four different seasons and shows clear seasonal patterns of the concentrations of OA fractions and total OAs, with higher and lower levels in summer and winter, respectively. HR–AMS data combined with PMF identified five factors and quantified their distributions among the three OA fractions: the MO-OOA, BBOA-like, BSOA-like, CROA, and HOA factors. The BSOA-like factor exhibited a pronounced seasonal pattern, peaking in summer and showing strong correlations with temperature and solar radiation. The BSOA-like factor was the dominant contributor to the HULIS fraction, accounting for 54.2 %.

In this work, a series of methods based on previous studies were developed to characterize the chemical structural information of different factors, especially for BBOA and BSOA. We identified several nonhydrocarbon ions, including $C_5H_6O^+$, $C_7H_9O_3^+$ and $C_9H_{13}O_4^+$, as potential BSOA-like compound markers. Despite their low signal intensities, these ions showed some specificity for the BSOA-like factor and could serve as markers of BSOA in future atmospheric research by EI mass spectrometry. This study also explored

CHN family ions as potential BBOA-like factor markers in AMS-based PMF for the first time to our knowledge, revealing a strong correlation on a mass fraction basis. By analyzing the three most abundant ions in the CHN family, CHN^+, CH_4N^+, and $C_2H_3N^+$, we interpreted their occurrence as indicating the emissions from protein-rich biomass combustion and the subsequent formation of CHN family species. In addition, we identified CROA factor, characterized by aromatic compounds, and considered their sources to be fossil fuel OAs and/or the combustion of aged biomass.

Finally, polarity-based analysis combined with PMF was performed. The BSOA-like PMF factor dominated in summer, whereas the BBOA-like, CROA, and HOA factors increased during colder seasons. HOA was almost water-insoluble, CROA was more hydrophobic than BBOA-like factor due to its aromatic composition, whereas BSOA-like and MO-OOA factors were mainly water soluble. A comparison across different sites revealed that compared with urban aerosols, forest aerosols had lower OA concentrations but higher proportions of HULIS. This difference is explained by the greater abundance of BSOA in forest environments, which were present mainly in the HULIS fraction.

Overall, the results of this study demonstrate that HR–AMS fragment ions help to distinguish sources such as BBOA and BSOA, providing potential markers for future EI-based mass spectrometric research. The results also highlight the importance of long-term observations and systematic analysis of the polarity-resolved source apportionment in advancing our understanding of the chemical complexity of OAs. In this study, the different distributions of the BBOA-like and BSOA-like factors among the three OA fractions demonstrate the distinction between these two structures. The PMF factors identified in this study are better interpreted as dynamic mixtures of submolecular structures rather than fixed sets of organic compounds. This is because OAs from respective sources would not have nearly-fixed mass spectra, given the aging of OA during transport. This may also be the case for the PMF factors reported in previous conventional online studies. Looking ahead, extending the source apportionment results based on chemical structural differences to investigations of the properties related to the roles of OA in climate and air quality would be valuable.

Data availability. The data for this study are presented in this manuscript and the supporting information material, and additional data will be available in the Zenodo data repository (https://doi.org/10.5281/zenodo.20610263, Sun et al., 2026).

Supplement. The supplement related to this article is available online at https://doi.org/10.5194/acp-26-12813-2026-supplement.

Author contributions. QS and MM jointly conceptualized the study and designed the experiments. LA, TP, SO, and MK contributed to the use of the SMEAR II station for aerosol sampling, and IJ, LA, TP, and MK to its use for BVOC measurements. QS and CS performed the experiments with contributions from RZ and MM. QS analyzed the data with contributions from MM and prepared the manuscript with contributions from MM, RZ, TP, and IJ.

Competing interests. At least one of the (co-)authors is a member of the editorial board of *Atmospheric Chemistry and Physics*. The peer-review process was guided by an independent editor, and the authors also have no other competing interests to declare.

Disclaimer. Publisher's note: Copernicus Publications remains neutral with regard to jurisdictional claims made in the text, published maps, institutional affiliations, or any other geographical representation in this paper. The authors bear the ultimate responsibility for providing appropriate place names. Views expressed in the text are those of the authors and do not necessarily reflect the views of the publisher.

Acknowledgements. The first author gratefully acknowledges support from the "Interdisciplinary Frontier Next-Generation Researcher Program" of the Tokai Higher Education and Research System. Funding through ACTRIS-IMP Transnational Access is gratefully acknowledged. The technical staff of SMEAR II are gratefully acknowledged for their support during measurements and sampling. The authors gratefully acknowledge NOAA''s Air Resources Laboratory (ARL) for providing the HYSPLIT transport and dispersion model and the READY website used in this study.

Financial support. This work was partly undertaken under JSPS KAKENHI (grant nos. JP23H00515, JP23H00525, and JP19KK0265), JST SPRING (grant no. JPMJSP2125), and a project of the Environment Research and Technology Development Fund of the ERCA (grant no. JPMEERF20262002). The operation of SMEAR II is financially supported by the University of Helsinki and Research Council of Finland through INAR RI (grant nos. 345510, 358647, 367739), projects (grant no. 377242), and ACCC flagship (grant nos. 337549, 357902, 359340, 374287).

Review statement. This paper was edited by Theodora Nah and reviewed by five anonymous referees.

References

Aalto, J., Aalto, P., Keronen, P., Kolari, P., Rantala, P., Taipale, R., Kajos, M., Patokoski, J., Rinne, J., Ruuskanen, T., Leskinen, M., Laakso, H., Levula, J., Pohja, T., Siivola, E., Kulmala, M., and Ylivinkka, I.: SMEAR II Hyytiälä forest meteorology, greenhouse gases, air quality and soil, FAIRDATA Etsin [data set], https://doi.org/10.23729/fd-933fd9fd-d31b-3e26-a01b-acef7901b843, 2025.

Afsana, S., Zhou, R., Miyazaki, Y., Tachibana, E., Deshmukh, D. K., Kawamura, K., and Mochida, M.: Abundance, chemical structure, and light absorption properties of humic-like substances (HULIS) and other organic fractions of forest aerosols in Hokkaido, Sci. Rep., 12, 14379, https://doi.org/10.1038/s41598-022-18201-z, 2022.

Äijälä, M., Heikkinen, L., Fröhlich, R., Canonaco, F., Prévôt, A. S. H., Junninen, H., Petäjä, T., Kulmala, M., Worsnop, D., and Ehn, M.: Resolving anthropogenic aerosol pollution types – deconvolution and exploratory classification of pollution events, Atmos. Chem. Phys., 17, 3165–3197, https://doi.org/10.5194/acp-17-3165-2017, 2017.

Äijälä, M., Daellenbach, K. R., Canonaco, F., Heikkinen, L., Junninen, H., Petäjä, T., Kulmala, M., Prévôt, A. S. H., and Ehn, M.: Constructing a data-driven receptor model for organic and inorganic aerosol – a synthesis analysis of eight mass spectrometric data sets from a boreal forest site, Atmos. Chem. Phys., 19, 3645–3672, https://doi.org/10.5194/acp-19-3645-2019, 2019.

Alfarra, M. R., Prevot, A. S. H., Szidat, S., Sandradewi, J., Weimer, S., Lanz, V. A., Schreiber, D., Mohr, M., and Baltensperger, U.: Identification of the Mass Spectral Signature of Organic Aerosols from Wood Burning Emissions, Environ. Sci. Technol., 41, 5770–5777, 10.1021/es062289b, 2007.

Andreae, M. O.: Soot Carbon and Excess Fine Potassium: Long-Range Transport of Combustion-Derived Aerosols, Science, 220, 1148–1151, https://doi.org/10.1126/science.220.4602.1148, 1983.

Bahreini, R., Keywood, M. D., Ng, N. L., Varutbangkul, V., Gao, S., Flagan, R. C., Seinfeld, J. H., Worsnop, D. R., and Jimenez, J. L.: Measurements of Secondary Organic Aerosol from Oxidation of Cycloalkenes, Terpenes, and m-Xylene Using an Aerodyne Aerosol Mass Spectrometer, Environ. Sci. Technol., 39, 5674–5688, https://doi.org/10.1021/es048061a, 2005.

Bateman, A. P., Nizkorodov, S. A., Laskin, J., and Laskin, A.: High-Resolution Electrospray Ionization Mass Spectrometry Analysis of Water-Soluble Organic Aerosols Collected with a Particle into Liquid Sampler, Anal. Chem., 82, 8010–8016, https://doi.org/10.1021/ac1014386, 2010.

Boyd, C. M., Sanchez, J., Xu, L., Eugene, A. J., Nah, T., Tuet, W. Y., Guzman, M. I., and Ng, N. L.: Secondary organic aerosol formation from the β-pinene+NO_3 system: effect of humidity and peroxy radical fate, Atmos. Chem. Phys., 15, 7497–7522, https://doi.org/10.5194/acp-15-7497-2015, 2015.

Bressi, M., Sciare, J., Ghersi, V., Mihalopoulos, N., Petit, J.-E., Nicolas, J. B., Moukhtar, S., Rosso, A., Féron, A., Bonnaire, N., Poulakis, E., and Theodosi, C.: Sources and geographical origins of fine aerosols in Paris (France), Atmos. Chem. Phys., 14, 8813–8839, https://doi.org/10.5194/acp-14-8813-2014, 2014.

Chen, Q., Ikemori, F., and Mochida, M.: Light Absorption and Excitation-Emission Fluorescence of Urban Organic Aerosol Components and Their Relationship to Chemical Structure, Environ. Sci. Technol., 50, 10859-10868, 10.1021/acs.est.6b02541, 2016a.

Chen, Q., Ikemori, F., Higo, H., Asakawa, D., and Mochida, M.: Chemical Structural Characteristics of HULIS and Other Fractionated Organic Matter in Urban Aerosols: Results from Mass Spectral and FT-IR Analysis, Environ. Sci. Technol., 50, 1721–1730, https://doi.org/10.1021/acs.est.5b05277, 2016b.

Chen, Q., Ikemori, F., Nakamura, Y., Vodicka, P., Kawamura, K., and Mochida, M.: Structural and Light-Absorption Characteristics of Complex Water-Insoluble Organic Mixtures in Urban Submicrometer Aerosols, Environ. Sci. Technol., 51, 8293–8303, https://doi.org/10.1021/acs.est.7b01630, 2017.

Chen, W., Yang, H., Chen, Y., Li, K., Xia, M., and Chen, H.: Influence of Biochar Addition on Nitrogen Transformation during Copyrolysis of Algae and Lignocellulosic Biomass, Environ. Sci. Technol., 52, 9514–9521, https://doi.org/10.1021/acs.est.8b02485, 2018.

Cheng, Y., Ma, Y., and Hu, D.: Tracer-based source apportioning of atmospheric organic carbon and the influence of anthropogenic emissions on secondary organic aerosol formation in Hong Kong, Atmos. Chem. Phys., 21, 10589–10608, https://doi.org/10.5194/acp-21-10589-2021, 2021.

Cheng, Y., He, K.-B., Du, Z.-Y., Engling, G., Liu, J.-M., Ma, Y.-L., Zheng, M., and Weber, R. J.: The characteristics of brown carbon aerosol during winter in Beijing, Atmos. Environ., 127, 355–364, https://doi.org/10.1016/j.atmosenv.2015.12.035, 2016.

Chhabra, P. S., Flagan, R. C., and Seinfeld, J. H.: Elemental analysis of chamber organic aerosol using an aerodyne high-resolution aerosol mass spectrometer, Atmos. Chem. Phys., 10, 4111–4131, https://doi.org/10.5194/acp-10-4111-2010, 2010.

Chhabra, P. S., Ng, N. L., Canagaratna, M. R., Corrigan, A. L., Russell, L. M., Worsnop, D. R., Flagan, R. C., and Seinfeld, J. H.: Elemental composition and oxidation of chamber organic aerosol, Atmos. Chem. Phys., 11, 8827–8845, https://doi.org/10.5194/acp-11-8827-2011, 2011.

Corrigan, A. L., Russell, L. M., Takahama, S., Äijälä, M., Ehn, M., Junninen, H., Rinne, J., Petäjä, T., Kulmala, M., Vogel, A. L., Hoffmann, T., Ebben, C. J., Geiger, F. M., Chhabra, P., Seinfeld, J. H., Worsnop, D. R., Song, W., Auld, J., and Williams, J.: Biogenic and biomass burning organic aerosol in a boreal forest at Hyytiälä, Finland, during HUMPPA-COPEC 2010, Atmos. Chem. Phys., 13, 12233–12256, https://doi.org/10.5194/acp-13-12233-2013, 2013.

Crippa, M., Canonaco, F., Lanz, V. A., Äijälä, M., Allan, J. D., Carbone, S., Capes, G., Ceburnis, D., Dall'Osto, M., Day, D. A., DeCarlo, P. F., Ehn, M., Eriksson, A., Freney, E., Hildebrandt Ruiz, L., Hillamo, R., Jimenez, J. L., Junninen, H., Kiendler-Scharr, A., Kortelainen, A.-M., Kulmala, M., Laaksonen, A., Mensah, A. A., Mohr, C., Nemitz, E., O'Dowd, C., Ovadnevaite, J., Pandis, S. N., Petäjä, T., Poulain, L., Saarikoski, S., Sellegri, K., Swietlicki, E., Tiitta, P., Worsnop, D. R., Baltensperger, U., and Prévôt, A. S. H.: Organic aerosol components derived from 25 AMS data sets across Europe using a consistent ME-2 based source apportionment approach, Atmos. Chem. Phys., 14, 6159–6176, https://doi.org/10.5194/acp-14-6159-2014, 2014.

Cubison, M. J., Ortega, A. M., Hayes, P. L., Farmer, D. K., Day, D., Lechner, M. J., Brune, W. H., Apel, E., Diskin, G. S., Fisher, J. A., Fuelberg, H. E., Hecobian, A., Knapp, D. J., Mikoviny, T., Riemer, D., Sachse, G. W., Sessions, W., Weber, R. J., Weinheimer, A. J., Wisthaler, A., and Jimenez, J. L.: Effects of aging on organic aerosol from open biomass burning smoke in aircraft and laboratory studies, Atmos. Chem. Phys., 11, 12049–12064, https://doi.org/10.5194/acp-11-12049-2011, 2011.

Deng, Y., Yai, H., Fujinari, H., Kawana, K., Nakayama, T., and Mochida, M.: Diurnal variation and size dependence of the hygroscopicity of organic aerosol at a forest site in

Wakayama, Japan: their relationship to CCN concentrations, Atmos. Chem. Phys., 19, 5889–5903, https://doi.org/10.5194/acp-19-5889-2019, 2019.

Deng, Y., Fujinari, H., Yai, H., Shimada, K., Miyazaki, Y., Tachibana, E., Deshmukh, D. K., Kawamura, K., Nakayama, T., Tatsuta, S., Cai, M., Xu, H., Li, F., Tan, H., Ohata, S., Kondo, Y., Takami, A., Hatakeyama, S., and Mochida, M.: Offline analysis of the chemical composition and hygroscopicity of submicrometer aerosol at an Asian outflow receptor site and comparison with online measurements, Atmos. Chem. Phys., 22, 5515–5533, https://doi.org/10.5194/acp-22-5515-2022, 2022.

Draxler, R. R.: HYSPLIT4 user's guide, NOAA Air Resources Laboratory, Silver Spring, MD, NOAA Tech. Memo. ERL ARL-230, https://www.arl.noaa.gov/documents/reports/arl-230.pdf (last access: 6 June 2024), 1999.

Draxler, R. R. and Hess, G. D.: Description of the HYSPLIT_4 modeling system, NOAA Air Resources Laboratory, Silver Spring, MD, NOAA Tech. Memo. ERL ARL-224, https://www.arl.noaa.gov/documents/reports/arl-224.pdf (last access: 6 June 2024), 1997.

Draxler, R. R. and Hess, G. D.: An overview of the HYSPLIT_4 modeling system of trajectories, dispersion, and deposition, Austr. Meteorol. Mag., 47, 295–308, 1998.

Duarte, R. M. B. O. and Duarte, A. C.: A critical review of advanced analytical techniques for water-soluble organic matter from atmospheric aerosols, TrAC-Trend. Anal. Chem., 30, 1659–1671, https://doi.org/10.1016/j.trac.2011.04.020, 2011.

Dusek, U., Hitzenberger, R., Kasper-Giebl, A., Kistler, M., Meijer, H. A. J., Szidat, S., Wacker, L., Holzinger, R., and Röckmann, T.: Sources and formation mechanisms of carbonaceous aerosol at a regional background site in the Netherlands: insights from a year-long radiocarbon study, Atmos. Chem. Phys., 17, 3233–3251, https://doi.org/10.5194/acp-17-3233-2017, 2017.

Finessi, E., Decesari, S., Paglione, M., Giulianelli, L., Carbone, C., Gilardoni, S., Fuzzi, S., Saarikoski, S., Raatikainen, T., Hillamo, R., Allan, J., Mentel, Th. F., Tiitta, P., Laaksonen, A., Petäjä, T., Kulmala, M., Worsnop, D. R., and Facchini, M. C.: Determination of the biogenic secondary organic aerosol fraction in the boreal forest by NMR spectroscopy, Atmos. Chem. Phys., 12, 941–959, https://doi.org/10.5194/acp-12-941-2012, 2012.

Fischer, L., Breitenlechner, M., Canaval, E., Scholz, W., Striednig, M., Graus, M., Karl, T. G., Petäjä, T., Kulmala, M., and Hansel, A.: First eddy covariance flux measurements of semivolatile organic compounds with the PTR3-TOF-MS, Atmos. Meas. Tech., 14, 8019–8039, https://doi.org/10.5194/amt-14-8019-2021, 2021.

Ge, X., Sun, Y., Trousdell, J., Chen, M., and Zhang, Q.: Enhancing characterization of organic nitrogen components in aerosols and droplets using high-resolution aerosol mass spectrometry, Atmos. Meas. Tech., 17, 423–439, https://doi.org/10.5194/amt-17-423-2024, 2024.

Gelencsér, A., May, B., Simpson, D., Sánchez-Ochoa, A., Kasper-Giebl, A., Puxbaum, H., Caseiro, A., Pio, C., and Legrand, M.: Source apportionment of $PM_{2.5}$ organic aerosol over Europe: Primary/secondary, natural/anthropogenic, and fossil/biogenic origin, J. Geophys. Res.-Atmos., 112, https://doi.org/10.1029/2006JD008094, 2007.

Gilardoni, S., Vignati, E., Cavalli, F., Putaud, J. P., Larsen, B. R., Karl, M., Stenström, K., Genberg, J., Henne, S., and Dentener, F.: Better constraints on sources of carbonaceous aerosols using a combined 14C – macro tracer analysis in a European rural background site, Atmos. Chem. Phys., 11, 5685–5700, https://doi.org/10.5194/acp-11-5685-2011, 2011.

Guenther, A. B., Jiang, X., Heald, C. L., Sakulyanontvittaya, T., Duhl, T., Emmons, L. K., and Wang, X.: The Model of Emissions of Gases and Aerosols from Nature version 2.1 (MEGAN2.1): an extended and updated framework for modeling biogenic emissions, Geosci. Model Dev., 5, 1471–1492, https://doi.org/10.5194/gmd-5-1471-2012, 2012.

Gysel, M., Weingartner, E., Nyeki, S., Paulsen, D., Baltensperger, U., Galambos, I., and Kiss, G.: Hygroscopic properties of water-soluble matter and humic-like organics in atmospheric fine aerosol, Atmos. Chem. Phys., 4, 35–50, https://doi.org/10.5194/acp-4-35-2004, 2004.

Hakola, H., Hellén, H., Hemmilä, M., Rinne, J., and Kulmala, M.: In situ measurements of volatile organic compounds in a boreal forest, Atmos. Chem. Phys., 12, 11665–11678, https://doi.org/10.5194/acp-12-11665-2012, 2012.

Haque, M. M., Verma, S. K., Deshmukh, D. K., Kunwar, B., and Kawamura, K.: Seasonal characteristics of biogenic secondary organic aerosol tracers in a deciduous broadleaf forest in northern Japan, Chemosphere, 311, 136785, https://doi.org/10.1016/j.chemosphere.2022.136785, 2023.

Heikkinen, L., Äijälä, M., Daellenbach, K. R., Chen, G., Garmash, O., Aliaga, D., Graeffe, F., Räty, M., Luoma, K., Aalto, P., Kulmala, M., Petäjä, T., Worsnop, D., and Ehn, M.: Eight years of sub-micrometre organic aerosol composition data from the boreal forest characterized using a machine-learning approach, Atmos. Chem. Phys., 21, 10081–10109, https://doi.org/10.5194/acp-21-10081-2021, 2021.

Heikkinen, L., Äijälä, M., Riva, M., Luoma, K., Dällenbach, K., Aalto, J., Aalto, P., Aliaga, D., Aurela, M., Keskinen, H., Makkonen, U., Rantala, P., Kulmala, M., Petäjä, T., Worsnop, D., and Ehn, M.: Long-term sub-micrometer aerosol chemical composition in the boreal forest: inter- and intra-annual variability, Atmos. Chem. Phys., 20, 3151–3180, https://doi.org/10.5194/acp-20-3151-2020, 2020.

Hellén, H., Praplan, A. P., Tykkä, T., Ylivinkka, I., Vakkari, V., Bäck, J., Petäjä, T., Kulmala, M., and Hakola, H.: Long-term measurements of volatile organic compounds highlight the importance of sesquiterpenes for the atmospheric chemistry of a boreal forest, Atmos. Chem. Phys., 18, 13839–13863, https://doi.org/10.5194/acp-18-13839-2018, 2018.

Hemmilä, M., Hellén, H., Virkkula, A., Makkonen, U., Praplan, A. P., Kontkanen, J., Ahonen, L., Kulmala, M., and Hakola, H.: Amines in boreal forest air at SMEAR II station in Finland, Atmos. Chem. Phys., 18, 6367–6380, https://doi.org/10.5194/acp-18-6367-2018, 2018.

Hennigan, C. J., Sullivan, A. P., Collett Jr., J. L., and Robinson, A. L.: Levoglucosan stability in biomass burning particles exposed to hydroxyl radicals, Geophys. Res. Lett., 37, https://doi.org/10.1029/2010GL043088, 2010.

Hu, W., Hu, M., Hu, W.-W., Zheng, J., Chen, C., Wu, Y., and Guo, S.: Seasonal variations in high time-resolved chemical compositions, sources, and evolution of atmospheric submicron aerosols in the megacity Beijing, Atmos. Chem. Phys., 17, 9979–10000, https://doi.org/10.5194/acp-17-9979-2017, 2017.

Hu, W. W., Campuzano-Jost, P., Palm, B. B., Day, D. A., Ortega, A. M., Hayes, P. L., Krechmer, J. E., Chen, Q., Kuwata, M., Liu, Y. J., de Sá, S. S., McKinney, K., Martin, S. T., Hu, M., Budisulistiorini, S. H., Riva, M., Surratt, J. D., St. Clair, J. M., Isaacman-Van Wertz, G., Yee, L. D., Goldstein, A. H., Carbone, S., Brito, J., Artaxo, P., de Gouw, J. A., Koss, A., Wisthaler, A., Mikoviny, T., Karl, T., Kaser, L., Jud, W., Hansel, A., Docherty, K. S., Alexander, M. L., Robinson, N. H., Coe, H., Allan, J. D., Canagaratna, M. R., Paulot, F., and Jimenez, J. L.: Characterization of a real-time tracer for isoprene epoxydiols-derived secondary organic aerosol (IEPOX-SOA) from aerosol mass spectrometer measurements, Atmos. Chem. Phys., 15, 11807–11833, https://doi.org/10.5194/acp-15-11807-2015, 2015.

Jeong, U., Kim, J., Lee, H., Jung, J., Kim, Y. J., Song, C. H., and Koo, J.-H.: Estimation of the contributions of long range transported aerosol in East Asia to carbonaceous aerosol and PM concentrations in Seoul, Korea using highly time resolved measurements: a PSCF model approach, J. Environ. Monit., 13, 1905–1918, https://doi.org/10.1039/C0EM00659A, 2011.

Jiang, J., Aksoyoglu, S., El-Haddad, I., Ciarelli, G., Denier van der Gon, H. A. C., Canonaco, F., Gilardoni, S., Paglione, M., Minguillón, M. C., Favez, O., Zhang, Y., Marchand, N., Hao, L., Virtanen, A., Florou, K., O'Dowd, C., Ovadnevaite, J., Baltensperger, U., and Prévôt, A. S. H.: Sources of organic aerosols in Europe: a modeling study using CAMx with modified volatility basis set scheme, Atmos. Chem. Phys., 19, 15247–15270, https://doi.org/10.5194/acp-19-15247-2019, 2019.

Jolleys, M. D., Coe, H., McFiggans, G., Taylor, J. W., O'Shea, S. J., Le Breton, M., Bauguitte, S. J.-B., Moller, S., Di Carlo, P., Aruffo, E., Palmer, P. I., Lee, J. D., Percival, C. J., and Gallagher, M. W.: Properties and evolution of biomass burning organic aerosol from Canadian boreal forest fires, Atmos. Chem. Phys., 15, 3077–3095, https://doi.org/10.5194/acp-15-3077-2015, 2015.

Junninen, H., Lauri, A., Keronen, P., Aalto, P., Hiltunen, V., Hari, P., and Kulmala, M.: Smart-SMEAR: on-line data exploration and visualization tool for SMEAR stations, Boreal Environ. Res., 14, 447–457, 2009.

Kiendler-Scharr, A., Zhang, Q., Hohaus, T., Kleist, E., Mensah, A., Mentel, T. F., Spindler, C., Uerlings, R., Tillmann, R., and Wildt, J.: Aerosol Mass Spectrometric Features of Biogenic SOA: Observations from a Plant Chamber and in Rural Atmospheric Environments, Environ. Sci. Technol., 43, 8166–8172, https://doi.org/10.1021/es901420b, 2009.

Kortelainen, A., Hao, L., Tiitta, P., Jaatinen, A., Miettinen, P., Kulmala, M., Smith, J. N., Laaksonen, A., Worsnop, D. R., and Virtanen, A.: Sources of particulate organic nitrates in the boreal forest in Finland, Boreal Environ. Res., 22, 13–26, 2017.

Kostenidou, E., Karnezi, E., Kolodziejczyk, A., Szmigielski, R., and Pandis, S. N.: Physical and Chemical Properties of 3-Methyl-1,2,3-butanetricarboxylic Acid (MBTCA) Aerosol, Environ. Sci. Technol., 52, 1150–1155, https://doi.org/10.1021/acs.est.7b04348, 2018.

Kuenen, J., Dellaert, S., Visschedijk, A., Jalkanen, J.-P., Super, I., and Denier van der Gon, H.: CAMS-REG-v4: a state-of-the-art high-resolution European emission inventory for air quality modelling, Earth Syst. Sci. Data, 14, 491–515, https://doi.org/10.5194/essd-14-491-2022, 2022.

Kulmala, M., Hämeri, K., Aalto, P. P., Mäkelä, J. M., Pirjola, L., Nilsson, E. D., Buzorius, G., Rannik, Ü., Dal Maso, M., Seidl, W., Hoffman, T., Janson, R., Hansson, H.-C., Viisanen, Y., Laaksonen, A., and O'Dowd, C. D.: Overview of the international project on biogenic aerosol formation in the boreal forest (BIOFOR), Tellus B, 53, 324–343, https://doi.org/10.1034/j.1600-0889.2001.530402.x, 2001.

Kunwar, B. and Kawamura, K.: One-year observations of carbonaceous and nitrogenous components and major ions in the aerosols from subtropical Okinawa Island, an outflow region of Asian dusts, Atmos. Chem. Phys., 14, 1819–1836, https://doi.org/10.5194/acp-14-1819-2014, 2014.

Kuuluvainen, T. and Aakala, T.: Natural forest dynamics in boreal Fennoscandia: a review and classification, Silva Fenn., 45, 823–841, 2011.

Laskin, A., Smith, J. S., and Laskin, J.: Molecular Characterization of Nitrogen-Containing Organic Compounds in Biomass Burning Aerosols Using High-Resolution Mass Spectrometry, Environ. Sci. Technol., 43, 3764–3771, https://doi.org/10.1021/es803456n, 2009.

Laskin, J., Laskin, A., Nizkorodov, S. A., Roach, P., Eckert, P., Gilles, M. K., Wang, B., Lee, H. J., and Hu, Q.: Molecular Selectivity of Brown Carbon Chromophores, Environ. Sci. Technol., 48, 12047–12055, https://doi.org/10.1021/es503432r, 2014.

Lee, T., Sullivan, A. P., Mack, L., Jimenez, J. L., Kreidenweis, S. M., Onasch, T. B., Worsnop, D. R., Malm, W., Wold, C. E., and Hao, W. M.: Chemical smoke marker emissions during flaming and smoldering phases of laboratory open burning of wildland fuels, Aerosol Sci. Tech., 44, https://doi.org/10.1080/02786826.2010.499884, 2010.

Li, L., Han, Y., Li, J., Lin, Y., Zhang, X., Wang, Q., and Cao, J.: Effects of photochemical aging on the molecular composition of organic aerosols derived from agricultural biomass burning in whole combustion process, Sci. Total Environ., 946, 174152, https://doi.org/10.1016/j.scitotenv.2024.174152, 2024.

Li, Y., Fu, T.-M., Yu, J. Z., Feng, X., Zhang, L., Chen, J., Boreddy, S. K. R., Kawamura, K., Fu, P., Yang, X., Zhu, L., and Zeng, Z.: Impacts of Chemical Degradation on the Global Budget of Atmospheric Levoglucosan and Its Use As a Biomass Burning Tracer, Environ. Sci. Technol., 55, 5525–5536, https://doi.org/10.1021/acs.est.0c07313, 2021.

Li, Y., Fu, T.-M., Yu, J. Z., Zhang, A., Yu, X., Ye, J., Zhu, L., Shen, H., Wang, C., Yang, X., Tao, S., Chen, Q., Li, Y., Li, L., Che, H., and Heald, C. L.: Nitrogen dominates global atmospheric organic aerosol absorption, Science, 387, 989–995, https://doi.org/10.1126/science.adr4473, 2025.

Liao, L., Dal Maso, M., Taipale, R., Rinne, J., Ehn, M., Junninen, H., Äijälä, M., Nieminen, T., Alekseychik, P., Hulkkonen, M., Worsnop, D. R., Kerminen, V.-M., and Kulmala, M.: Monoterpene pollution episodes in a forest environment: indication of anthropogenic origin and association with aerosol particles, Boreal Environ. Res., 16, 288–303, 2011.

Lin, P., Huang, X.-F., He, L.-Y., and Zhen Yu, J.: Abundance and size distribution of HULIS in ambient aerosols at a rural site in South China, J. Aerosol Sci., 41, 74–87, https://doi.org/10.1016/j.jaerosci.2009.09.001, 2010.

Liu, C., Chung, C. E., Zhang, F., and Yin, Y.: The colors of biomass burning aerosols in the atmosphere, Sci. Rep., 6, 28267, https://doi.org/10.1038/srep28267, 2016.

Ma, Y.-J., Xu, Y., Yang, T., Xiao, H.-W., and Xiao, H.-Y.: Measurement report: Characteristics of nitrogen-containing organics in $PM_{2.5}$ in Ürümqi, northwestern China – differential impacts of combustion of fresh and aged biomass materials, Atmos. Chem. Phys., 24, 4331–4346, https://doi.org/10.5194/acp-24-4331-2024, 2024.

McLafferty, F. W. and Turecek, F.: Interpretation of mass spectra, University Science Books, ISBN 978-0-935702-25-5, 1993.

Mihara, T. and Mochida, M.: Characterization of Solvent-Extractable Organics in Urban Aerosols Based on Mass Spectrum Analysis and Hygroscopic Growth Measurement, Environ. Sci. Technol., 45, 9168–9174, https://doi.org/10.1021/es201271w, 2011.

Mochida, M., Kawamura, K., Fu, P., and Takemura, T.: Seasonal variation of levoglucosan in aerosols over the western North Pacific and its assessment as a biomass-burning tracer, Atmos. Environ., 44, 3511–3518, https://doi.org/10.1016/j.atmosenv.2010.06.017, 2010.

Müller, A., Aoki, K., Tachibana, E., Hiura, T., and Miyazaki, Y.: Impact of biogenic emissions of organic matter from a cool-temperate forest on aerosol optical properties, Atmos. Environ., 229, 117413, https://doi.org/10.1016/j.atmosenv.2020.117413, 2020.

Ng, N. L., Canagaratna, M. R., Zhang, Q., Jimenez, J. L., Tian, J., Ulbrich, I. M., Kroll, J. H., Docherty, K. S., Chhabra, P. S., Bahreini, R., Murphy, S. M., Seinfeld, J. H., Hildebrandt, L., Donahue, N. M., DeCarlo, P. F., Lanz, V. A., Prévôt, A. S. H., Dinar, E., Rudich, Y., and Worsnop, D. R.: Organic aerosol components observed in Northern Hemispheric datasets from Aerosol Mass Spectrometry, Atmos. Chem. Phys., 10, 4625–4641, https://doi.org/10.5194/acp-10-4625-2010, 2010.

Nguyen, Q. T., Christensen, M. K., Cozzi, F., Zare, A., Hansen, A. M. K., Kristensen, K., Tulinius, T. E., Madsen, H. H., Christensen, J. H., Brandt, J., Massling, A., Nøjgaard, J. K., and Glasius, M.: Understanding the anthropogenic influence on formation of biogenic secondary organic aerosols in Denmark via analysis of organosulfates and related oxidation products, Atmos. Chem. Phys., 14, 8961–8981, https://doi.org/10.5194/acp-14-8961-2014, 2014.

Petäjä, T., Tabakova, K., Manninen, A., Ezhova, E., O'Connor, E., Moisseev, D., Sinclair, V. A., Backman, J., Levula, J., Luoma, K., Virkkula, A., Paramonov, M., Räty, M., Äijälä, M., Heikkinen, L., Ehn, M., Sipilä, M., Yli-Juuti, T., Virtanen, A., Ritsche, M., Hickmon, N., Pulik, G., Rosenfeld, D., Worsnop, D. R., Bäck, J., Kulmala, M., and Kerminen, V. M.: Influence of biogenic emissions from boreal forests on aerosol–cloud interactions, Nat. Geosci., 15, 42–47, https://doi.org/10.1038/s41561-021-00876-0, 2021.

Qin, M., Hu, Y., Wang, X., Vasilakos, P., Boyd, C. M., Xu, L., Song, Y., Ng, N. L., Nenes, A., and Russell, A. G.: Modeling biogenic secondary organic aerosol (BSOA) formation from monoterpene reactions with NO_3: A case study of the SOAS campaign using CMAQ, Atmos. Environ., 184, 146–155, https://doi.org/10.1016/j.atmosenv.2018.03.042, 2018.

Raatikainen, T., Vaattovaara, P., Tiitta, P., Miettinen, P., Rautiainen, J., Ehn, M., Kulmala, M., Laaksonen, A., and Worsnop, D. R.: Physicochemical properties and origin of organic groups detected in boreal forest using an aerosol mass spectrometer, Atmos. Chem. Phys., 10, 2063–2077, https://doi.org/10.5194/acp-10-2063-2010, 2010.

Ratcliff Jr., M. A., Medley, E. E., and Simmonds, P. G.: Pyrolysis of amino acids. Mechanistic considerations, J. Organic Chem., 39, 1481–1490, https://doi.org/10.1021/jo00924a007, 1974.

Riuttanen, L., Hulkkonen, M., Dal Maso, M., Junninen, H., and Kulmala, M.: Trajectory analysis of atmospheric transport of fine particles, SO_2, NO_x and O_3 to the SMEAR II station in Finland in 1996–2008, Atmos. Chem. Phys., 13, 2153–2164, https://doi.org/10.5194/acp-13-2153-2013, 2013.

Robinson, N. H., Hamilton, J. F., Allan, J. D., Langford, B., Oram, D. E., Chen, Q., Docherty, K., Farmer, D. K., Jimenez, J. L., Ward, M. W., Hewitt, C. N., Barley, M. H., Jenkin, M. E., Rickard, A. R., Martin, S. T., McFiggans, G., and Coe, H.: Evidence for a significant proportion of Secondary Organic Aerosol from isoprene above a maritime tropical forest, Atmos. Chem. Phys., 11, 1039–1050, https://doi.org/10.5194/acp-11-1039-2011, 2011.

Ronold, E. K., Morgado, L., Mundra, S., Nybakken, L., Halvorsen, R., and Kauserud, H.: Above- and belowground communities in boreal forests are tightly linked along common ecological gradients, Plant Soil, 521, 1231–1251, https://doi.org/10.1007/s11104-026-08440-8, 2026.

Schauer, J. J., Rogge, W. F., Hildemann, L. M., Mazurek, M. A., Cass, G. R., and Simoneit, B. R. T.: Source apportionment of airborne particulate matter using organic compounds as tracers, Atmos. Environ., 30, 3837–3855, https://doi.org/10.1016/1352-2310(96)00085-4, 1996.

Seinfeld, J. H. and Pandis, S. N.: Atmospheric chemistry and physics: from air pollution to climate change, John Wiley & Sons, ISBN 978-1-118-94740-1, 2016.

Simoneit, B. R. T.: Biomass burning – a review of organic tracers for smoke from incomplete combustion, Appl. Geochem., 17, 129–162, https://doi.org/10.1016/S0883-2927(01)00061-0, 2002.

Simoneit, B. R. T., Rushdi, A. I., bin Abas, M. R., and Didyk, B. M.: Alkyl Amides and Nitriles as Novel Tracers for Biomass Burning, Environ. Sci. Technol., 37, 16–21, https://doi.org/10.1021/es020811y, 2003.

Sipilä, M., Sarnela, N., Jokinen, T., Junninen, H., Hakala, J., Rissanen, M. P., Praplan, A., Simon, M., Kürten, A., Bianchi, F., Dommen, J., Curtius, J., Petäjä, T., and Worsnop, D. R.: Bisulfate – cluster based atmospheric pressure chemical ionization mass spectrometer for high-sensitivity (< 100 ppqV) detection of atmospheric dimethyl amine: proof-of-concept and first ambient data from boreal forest, Atmos. Meas. Tech., 8, 4001–4011, https://doi.org/10.5194/amt-8-4001-2015, 2015.

Srivastava, D., Favez, O., Perraudin, E., Villenave, E., and Albinet, A.: Comparison of Measurement-Based Methodologies to Apportion Secondary Organic Carbon (SOC) in $PM_{2.5}$: A Review of Recent Studies, Atmosphere, 9, 452, https://doi.org/10.3390/atmos9110452, 2018.

Stein, A. F., Draxler, R. R., Rolph, G. D., Stunder, B. J. B., Cohen, M. D., and Ngan, F.: NOAA's HYSPLIT atmospheric transport and dispersion modeling system, B. Am. Meteorol. Soc., 96, 2059–2077, https://doi.org/10.1175/BAMS-D-14-00110.1, 2015.

Sun, Y., Jiang, Q., Xu, Y., Ma, Y., Zhang, Y., Liu, X., Li, W., Wang, F., Li, J., Wang, P., and Li, Z.: Aerosol characterization

over the North China Plain: Haze life cycle and biomass burning impacts in summer, J. Geophys. Res.-Atmos., 121, 2508–2521, https://doi.org/10.1002/2015JD024261, 2016.

Sun, Q., Zhou, R., Ohata, S., Petäjä, T., Ahonen, L., Kulmala, M., and Mochida, M.: Dataset for unraveling the chemical structures and sources of biomass-derived organic aerosols through a year-long offline analysis in Hyytiälä, Finland, Zenodo [data set]. https://doi.org/10.5281/zenodo.20610263, 2026.

Szidat, S., Jenk, T. M., Synal, H.-A., Kalberer, M., Wacker, L., Hajdas, I., Kasper-Giebl, A., and Baltensperger, U.: Contributions of fossil fuel, biomass-burning, and biogenic emissions to carbonaceous aerosols in Zurich as traced by ^{14}C, J. Geophys. Res.-Atmos., 111, https://doi.org/10.1029/2005JD006590, 2006.

Tarvainen, V., Hakola, H., Hellén, H., Bäck, J., Hari, P., and Kulmala, M.: Temperature and light dependence of the VOC emissions of Scots pine, Atmos. Chem. Phys., 5, 989–998, https://doi.org/10.5194/acp-5-989-2005, 2005.

Tunved, P., Hansson, H.-C., Kerminen, V.-M., Ström, J., Dal Maso, M., Lihavainen, H., Viisanen, Y., Aalto, P. P., Komppula, M., and Kulmala, M.: High Natural Aerosol Loading over Boreal Forests, Science, 312, 261–263, https://doi.org/10.1126/science.1123052, 2006.

Ulbrich, I. M., Canagaratna, M. R., Zhang, Q., Worsnop, D. R., and Jimenez, J. L.: Interpretation of organic components from Positive Matrix Factorization of aerosol mass spectrometric data, Atmos. Chem. Phys., 9, 2891–2918, https://doi.org/10.5194/acp-9-2891-2009, 2009a.

Ulbrich, I. M., Handschy, A., Lechner, M., and Jimenez, J. L.: AMS Spectral Database, University of Colorado Boulder [data set], http://cires.colorado.edu/jimenez-group/AMSsd/ (last access: 16 April 2025), 2009b.

Varga, B., Kiss, G., Ganszky, I., Gelencsér, A., and Krivácsy, Z.: Isolation of water-soluble organic matter from atmospheric aerosol, Talanta, 55, 561–572, https://doi.org/10.1016/S0039-9140(01)00446-5, 2001.

Vogel, A. L., Äijälä, M., Corrigan, A. L., Junninen, H., Ehn, M., Petäjä, T., Worsnop, D. R., Kulmala, M., Russell, L. M., Williams, J., and Hoffmann, T.: In situ submicron organic aerosol characterization at a boreal forest research station during HUMPPA-COPEC 2010 using soft and hard ionization mass spectrometry, Atmos. Chem. Phys., 13, 10933–10950, https://doi.org/10.5194/acp-13-10933-2013, 2013.

Wang, S., Pavuluri, C. M., Ren, L., Fu, P., Zhang, Y.-L., and Liu, C.-Q.: Implications for biomass/coal combustion emissions and secondary formation of carbonaceous aerosols in North China, RSC Advances, 8, 38108–38117, https://doi.org/10.1039/C8RA06127K, 2018.

Williams, J., Crowley, J., Fischer, H., Harder, H., Martinez, M., Petäjä, T., Rinne, J., Bäck, J., Boy, M., Dal Maso, M., Hakala, J., Kajos, M., Keronen, P., Rantala, P., Aalto, J., Aaltonen, H., Paatero, J., Vesala, T., Hakola, H., Levula, J., Pohja, T., Herrmann, F., Auld, J., Mesarchaki, E., Song, W., Yassaa, N., Nölscher, A., Johnson, A. M., Custer, T., Sinha, V., Thieser, J., Pouvesle, N., Taraborrelli, D., Tang, M. J., Bozem, H., Hosaynali-Beygi, Z., Axinte, R., Oswald, R., Novelli, A., Kubistin, D., Hens, K., Javed, U., Trawny, K., Breitenberger, C., Hidalgo, P. J., Ebben, C. J., Geiger, F. M., Corrigan, A. L., Russell, L. M., Ouwersloot, H. G., Vilà-Guerau de Arellano, J., Ganzeveld, L., Vogel, A., Beck, M., Bayerle, A., Kampf, C. J., Bertelmann, M., Köllner, F., Hoffmann, T., Valverde, J., González, D., Riekkola, M.-L., Kulmala, M., and Lelieveld, J.: The summertime Boreal forest field measurement intensive (HUMPPA-COPEC-2010): an overview of meteorological and chemical influences, Atmos. Chem. Phys., 11, 10599–10618, https://doi.org/10.5194/acp-11-10599-2011, 2011.

Xu, L., Guo, H., Weber, R. J., and Ng, N. L.: Chemical Characterization of Water-Soluble Organic Aerosol in Contrasting Rural and Urban Environments in the Southeastern United States, Environ. Sci. Technol., 51, 78–88, https://doi.org/10.1021/acs.est.6b05002, 2017.

Yan, C., Nie, W., Äijälä, M., Rissanen, M. P., Canagaratna, M. R., Massoli, P., Junninen, H., Jokinen, T., Sarnela, N., Häme, S. A. K., Schobesberger, S., Canonaco, F., Yao, L., Prévôt, A. S. H., Petäjä, T., Kulmala, M., Sipilä, M., Worsnop, D. R., and Ehn, M.: Source characterization of highly oxidized multifunctional compounds in a boreal forest environment using positive matrix factorization, Atmos. Chem. Phys., 16, 12715–12731, https://doi.org/10.5194/acp-16-12715-2016, 2016.

Yasmeen, F., Szmigielski, R., Vermeylen, R., Gómez-González, Y., Surratt, J. D., Chan, A. W. H., Seinfeld, J. H., Maenhaut, W., and Claeys, M.: Mass spectrometric characterization of isomeric terpenoic acids from the oxidation of α-pinene, β-pinene, d-limonene, and Δ3-carene in fine forest aerosol, J. Mass Spectrom., 46, 425-442, https://doi.org/10.1002/jms.1911, 2011.

Yin, J., Cumberland, S. A., Harrison, R. M., Allan, J., Young, D. E., Williams, P. I., and Coe, H.: Receptor modelling of fine particles in southern England using CMB including comparison with AMS-PMF factors, Atmos. Chem. Phys., 15, 2139–2158, https://doi.org/10.5194/acp-15-2139-2015, 2015.

Ylivinkka, I., Di Natale, C., Mikkelsen, M. K., Nissinen, A., Pennacchio, L., Strömberg, J., Saranko, O., Utriainen, L., Valiati, R., Aalto, J., Banerji, S., Heikkinen, L., Lintunen, A., Luoma, K., Peräkylä, O., Sarnela, N., Taipale, D., Taipale, R., Thomas, S. J., Zhang, X., and Kulmala, M.: Intervention of pollution episodes from nearby sawmills to ecosystem-atmosphere interactions studied in a boreal forest at SMEAR II, Boreal Environ. Res., 30, 221–241, https://doi.org/10.60910/ber2025.727e-sw95, 2025.

Yttri, K. E., Simpson, D., Nøjgaard, J. K., Kristensen, K., Genberg, J., Stenström, K., Swietlicki, E., Hillamo, R., Aurela, M., Bauer, H., Offenberg, J. H., Jaoui, M., Dye, C., Eckhardt, S., Burkhart, J. F., Stohl, A., and Glasius, M.: Source apportionment of the summer time carbonaceous aerosol at Nordic rural background sites, Atmos. Chem. Phys., 11, 13339–13357, https://doi.org/10.5194/acp-11-13339-2011, 2011.

Zhang, Q., Alfarra, M. R., Worsnop, D. R., Allan, J. D., Coe, H., Canagaratna, M. R., and Jimenez, J. L.: Deconvolution and Quantification of Hydrocarbon-like and Oxygenated Organic Aerosols Based on Aerosol Mass Spectrometry, Environ. Sci. Technol., 39, 4938–4952, https://doi.org/10.1021/es048568l, 2005.

Zhang, Q., Jimenez, J. L., Canagaratna, M. R., Ulbrich, I. M., Ng, N. L., Worsnop, D. R., and Sun, Y.: Understanding atmospheric organic aerosols via factor analysis of aerosol mass spectrometry: a review, Anal. Bioanal. Chem., 401, 3045-3067, https://doi.org/10.1007/s00216-011-5355-y, 2011.

Zhang, T., Shen, Z., Huang, S., Lei, Y., Zeng, Y., Sun, J., Zhang, Q., Ho, S. S. H., Xu, H., and Cao, J.: Optical properties, molec-

ular characterizations, and oxidative potentials of different polarity levels of water-soluble organic matters in winter $PM_{2.5}$ in six China's megacities, Sci. Total Environ., 853, 158600, https://doi.org/10.1016/j.scitotenv.2022.158600, 2022.

Zhang, X., Hecobian, A., Zheng, M., Frank, N. H., and Weber, R. J.: Biomass burning impact on PM 2.5 over the southeastern US during 2007: integrating chemically speciated FRM filter measurements, MODIS fire counts and PMF analysis, Atmos. Chem. Phys., 10, 6839–6853, https://doi.org/10.5194/acp-10-6839-2010, 2010.

Zhang, Y., Heikkinen, L., Äijälä, M., Peräkylä, O., Graeffe, F., Mickwitz, V., Zhao, J., Daellenbach, K., Sueper, D., Worsnop, D., Riva, M., and Ehn, M.: Enhanced Aerosol Source Identification by Utilizing High Molecular Weight Signals in Aerosol Mass Spectra, ACS ES&T Air, 1, 502–510, https://doi.org/10.1021/acsestair.3c00102, 2024.

Zheng, Y., Horowitz, L. W., Menzel, R., Paynter, D. J., Naik, V., Li, J., and Mao, J.: Anthropogenic amplification of biogenic secondary organic aerosol production, Atmos. Chem. Phys., 23, 8993–9007, https://doi.org/10.5194/acp-23-8993-2023, 2023.

Zhou, R., Chen, Q., Chen, J., Ren, L., Deng, Y., Vodicka, P., Deshmukh, D. K., Kawamura, K., Fu, P., and Mochida, M.: Distinctive Sources Govern Organic Aerosol Fractions with Different Degrees of Oxygenation in the Urban Atmosphere, Environ. Sci. Technol., 55, 4494–4503, https://doi.org/10.1021/acs.est.0c08604, 2021.